ACS Chemical Neuroscience

pubs.acs.org/chemneuro Research Article

Further Studies on Triazinoindoles as Potential Novel Multitarget-Directed Anti-Alzheimer's Agents

Dushyant V. Patel, Nirav R. Patel, Ashish M. Kanhed, Divya M. Teli, Kishan B. Patel, Pallav M. Gandhi, Sagar P. Patel, Bharat N. Chaudhary, Dharti B. Shah, Navnit K. Prajapati, Kirti V. Patel, and Mange Ram Yadav*

Cite This: https://dx.doi.org/10.1021/acschemneuro.0c00448 Read Online

ACCESS | Metrics & More | Article Recommendations | Supporting Information

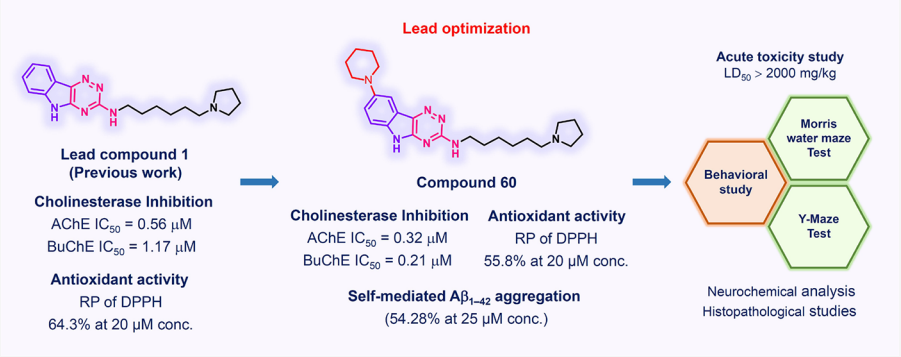

ABSTRACT: The inadequate clinical efficacy of the present anti-Alzheimer's disease (AD) drugs and their low impact on the progression of Alzheimer's disease in patients have revised the research focus from single targets to multitarget-directed ligands. A novel series of substituted triazinoindole derivatives were obtained by introducing various substituents on the indole ring for the development of multitarget-directed ligands as anti-AD agents. The experimental data indicated that some of these compounds exhibited significant anti-AD properties. Among them, 8-(piperidin-1-yl)-*N*-(6-(pyrrolidin-1-yl)hexyl)-5*H*-[1,2,4]triazino[5,6-*b*]indol-3-amine (**60**), the most potent cholinesterase inhibitor (AChE, IC_{50} value of 0.32 μM; BuChE, IC_{50} value of 0.21 μM), was also found to possess significant self-mediated $A\beta_{1-42}$ aggregation inhibitory activity (54% at 25 μM concentration). Additionally, compound **60** showed strong antioxidant activity. In the PAMPA assay, compound **60** exhibited blood-brain barrier penetrating ability. An acute toxicity study in rats demonstrated no sign of toxicity at doses up to 2000 mg/kg. Furthermore, compound **60** significantly restored the cognitive deficits in the scopolamine-induced mice model and $A\beta_{1-42}$-induced rat model. In the *in silico* ADMET prediction studies, the compound satisfied all the parameters of CNS acting drugs. These results highlighted the potential of compound **60** to be a promising multitarget-directed ligand for the development of potential anti-AD drugs.

KEYWORDS: *Alzheimer's disease, MTDL, acetylcholinesterase, butyrylcholinesterase, Aβ aggregation, triazinoindole, DPPH*

1. INTRODUCTION

Alzheimer's disease (AD) is a progressive neurodegenerative disorder, characterized by irreversible cognitive impairment, language deterioration, and severe behavioral abnormalities which ultimately leads to death.[1] It is the most prevailing form of age-related dementia. Today, around 50 million people worldwide live with dementia, and this number is reckoned to rise to 150 million by 2050 if no suitable medication is made available.[2] The pathogenesis of AD is highly complicated and not thoroughly understood; various factors like low levels of acetylcholine (ACh),[3] accumulation of the abnormal β-amyloid ($A\beta$) peptide,[4] oxidative stress,[5] hyperphosphorylation of tau protein,[6] and biometal dyshomeostasis[7] are contemplated to impart significant roles in the AD pathophysiology. At the present, therapeutic options available for the treatment of AD are limited to three cholinesterase (ChE) inhibitors (donepezil, rivastigmine, and galantamine) and one *N*-methyl-D-aspartate (NMDA) receptor antagonist (memantine).[8] They merely provide a symptomatic cure to the patient, while none of them is able to halt the progressive neurodegeneration that makes the AD debilitating and fatal.

The cholinergic hypothesis, the first theory proposed to elucidate the etiology of AD, outlines that the cognitive decline

Received: July 17, 2020
Accepted: October 7, 2020

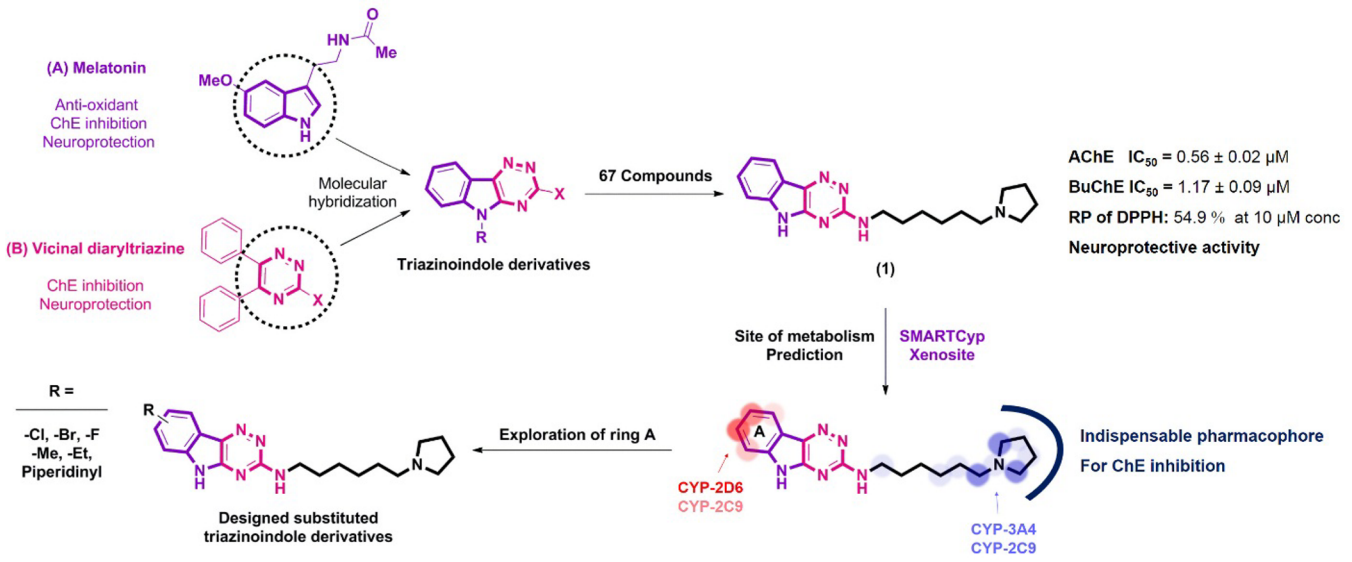

Figure 1. Rational design of substituted triazinoindole derivatives for the treatment of AD.

in AD is because of cholinergic system impairment. ACh plays an influential role in cognitive functions, particularly in memory. ACh is rapidly hydrolyzed by acetylcholinesterase (AChE) as well as by butyrylcholinesterase (BuChE). Declined levels of ACh are found in the AD patients' brains.[3,9] Hence, ChE inhibition remains a competent way to increase the levels of ACh within the brain.[10] Apart from its catalytical role, AChE also plays a proaggregatory role by stimulating Aβ aggregation and deposition in the fibrils. It is observed that AChE binds to the nonamyloidogenic form of Aβ through its peripheral anionic site (PAS) and induces conformational changes to the amyloidogenic form of Aβ with subsequent Aβ fibril formation.[11] In the advanced stages of AD, declining levels of AChE with a constant or increased levels of BuChE were observed.[12] BuChE performs staggered roles both in neural as well as non-neural functioning. High levels of BuChE in the brain are linked with certain characteristic AD traits, such as extracellular accumulation of the Aβ and intraneuronal hyperphosphorylated tau protein aggregations.[13] This signifies that both of the cholinesterases play an influential role in AD etiology. So, the designed multitarget-directed ligands (MTDLs) should act not only on AChE but also on BuChE.

It is well-known that the accumulation of the neurotoxic Aβ peptide in the brain is a major contributing factor in the pathogenesis of AD.[14,15] The Aβ plaques are the aggregated oligomeric Aβ of different lengths which are formed by the sequential action of the proteolytic enzymes β- and γ-secretase on amyloid precursor protein (APP). Among them, Aβ_{1-42} exhibits a high tendency to form fibrils and aggregates that are neurotoxic, and they continuously activate inflammatory mediators. Furthermore, Aβ_{1-42} itself serves as an oxygen-free radical donor generating reactive oxygen species (ROS) and affecting the general physiological functioning of neuronal cells.[16,17] Therefore, inhibition of Aβ_{1-42} aggregation can emerge as a plausible way to resolve AD.

Several converging lines of evidence show that oxidative stress appears ahead of any other hallmark of AD. The imbalance between the production and neutralization of free radicals leads to disturbance in the equilibration which induces oxidative stress.[18] The reactive oxygen species (ROS) and reactive nitrogen species (RNS) generated by pathological oxidation−reduction steps can vitiate the biomolecules such as lipids, proteins, and nucleic acids which ultimately lead to tissue damage through apoptosis and necrosis.[19] Thus, antioxidants having additional anti-AD activities are preferred to deal with this intricate disease, in which free radicals play a crucial role but are not the sole drivers.

In our previous work, a series of novel triazino[2,3-*b*]indoles as MTDLs, designed by molecular hybridization of diaryltriazine and melatonin, have been reported for the treatment of AD.[20] These derivatives displayed notable *in vitro* ChE inhibitory, antioxidant, and neuroprotective activities. Their fascinating biological profile encouraged us to further modify the triazino[2,3-*b*]indole scaffold. These synthesized derivatives were assessed for their multifactorial anti-AD activities including ChE inhibition, Aβ aggregation inhibition, antioxidant, *in vivo* anti-AD efficacy, and acute toxicity in animal models. Molecular modeling studies were performed to visualize more closely the binding mode of the most promising compound with the target proteins. ADMET properties of the most promising compound were also predicted computationally.

2. RATIONALE OF DESIGNING

In continuation of our research program to identify novel potential MTDLs to mitigate AD, a series of novel triazinoindole derivatives were reported in our previous work.[20] The most active compound (**1**) in the series exhibited significant cholinesterase inhibitory activity (IC_{50} value of 0.56 μM and 1.17 μM for AChE and BuChE, respectively) and excellent antioxidant and neuroprotective activities. It showed notable blood-brain barrier (BBB) permeability and improvement in memory deficit in AD animal models. To further improve the biological profile of compound **1**, some rational modifications were done in its structure, leading to the synthesis of a series of compounds which are presented in this report.

It is reported that the metabolism of triazinoindole derivatives occurs preferentially at the C8 position of the triazinoindole scaffold resulting in compounds that could be eliminated rapidly.[21] To identify the metabolically active sites, *in silico* prediction was done for the common "sites of

https://dx.doi.org/10.1021/acschemneuro.0c00448
ACS Chem. Neurosci. XXXX, XXX, XXX−XXX

Scheme 1. General Synthetic Route for the Synthesis of Substituted *N*-(Aminoalkyl)-5*H*-[1,2,4]triazino[5,6-*b*]indol-3-amine Derivatives (51−61)[a]

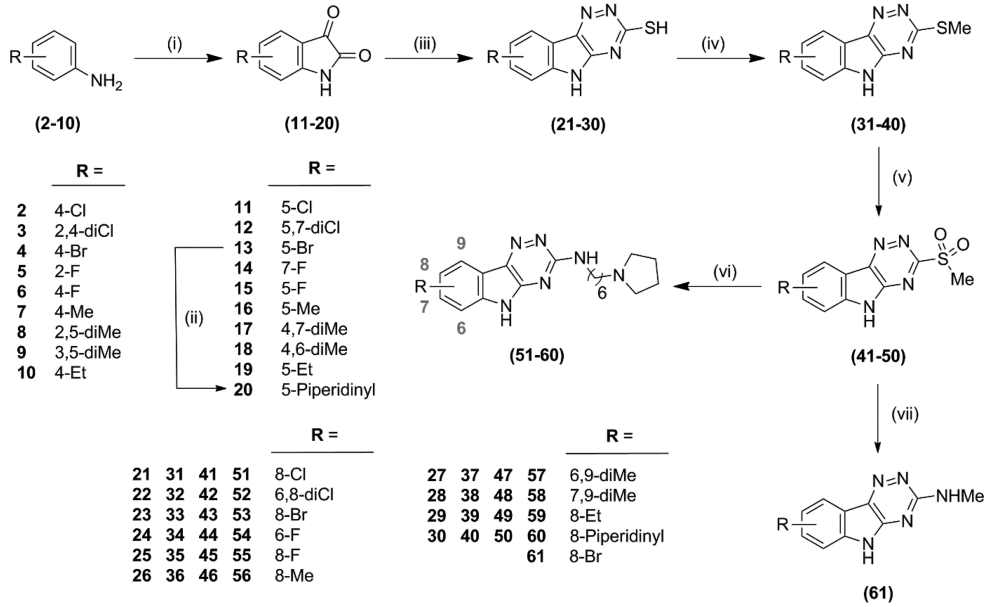

[a]Reagents and conditions: (i) (a) chloral hydrate, sodium sulfate, hydroxylamine HCl, (b) sulfuric acid, 80 °C; (ii) piperidine, K_2CO_3, DMF, 80 °C; (iii) thiosemicarbazide, K_2CO_3, H_2O, reflux, overnight; (iv) MeI, K_2CO_3, DMF. (v) *m*CPBA, DCM, 0 °C to RT; (vi) 6-(pyrrolidin-1-yl)hexan-1-amine, THF, reflux; (vii) methylamine, THF, reflux.

metabolism" (SOM) for compound **1** by SMARTCyp[22,23] and XenoSite tools.[24] The phenyl ring and alicyclic amine ring appeared to be the two main SOM in compound **1** as shown in Figure 1. Previous SAR studies have revealed that the alicyclic amine ring remains an indispensable pharmacophore for the cholinesterase inhibitory activity, as alteration or removal of it was found to be unfavorable to the ChE inhibitory activity. So, in the present work, we aimed to introduce some substituents, i.e., chloro, bromo, fluoro, methyl, ethyl, and piperidinyl, on the phenyl ring of the triazinoindole scaffold keeping in mind that the presence of at least one substituent in this ring not only would lower the metabolic susceptibility of the ring but also would enhance molecular interactions of the designed compounds with ChEs. Accordingly, a series of substituted triazinoindole derivatives as depicted in Figure 1 were synthesized and described here in this report.

3. RESULTS AND DISCUSSION

3.1. Chemistry. The designed substituted 5*H*-[1,2,4]-triazino[5,6-*b*]indol-3-amine derivatives (**51−61**) were synthesized from substituted isatins as depicted in Scheme 1. Substituted isatin derivatives (**11−19**) were synthesized by the Sandmeyer process of isatin synthesis.[25] Condensation of substituted anilines (**2−10**) with chloral hydrate and hydroxylamine to α-isonitrosoacetanilide and subsequent cyclization of the latter in the presence of concentrated sulfuric acid resulted in substituted isatins (**11−19**). 5-(Piperidin-1-yl)isatin (**20**) was synthesized by the reaction of piperidine with 5-bromoisatin (**13**) in the presence of potassium carbonate in DMF.[26] The reaction of pyrrolidine and diethylamine with 5-bromoisatin (**13**) failed to yield the respective 5-substituted isatins. Thiol derivatives (**21−30**) were obtained by condensation of these substituted isatins (**11−20**) and thiosemicarbazide in aqueous potassium carbonate solution at reflux conditions. Acidification of the resultant clear liquid by acetic acid afforded condensed products (**21−30**). These thiol derivatives were methylated by methyl iodide to get thiomethyl derivatives (**31−40**). Oxidation of the thiomethyl group at the C3 position of compounds (**31−40**) by *m*-chloroperbenzoic acid afforded sulfone derivatives (**41−50**). Reaction of these sulfone derivatives with 6-(pyrrolidin-1-yl)hexan-1-amine in THF solvent under refluxing conditions yielded the desired substituted [1,2,4]triazino[5,6-*b*]indol-3-amine derivatives (**51−60**). The required amine side chain, 6-(pyrrolidin-1-yl)hexan-1-amine, was synthesized from phthalimide by the Gabriel synthesis.[20] Synthesis of 8-bromo-*N*-methyl-5*H*-[1,2,4]triazino[5,6-*b*]indol-3-amine (**61**) was carried out by the reaction of sulfone (**43**) with methylamine.

3.2. Biological Evaluation. *3.2.1. In Vitro Cholinesterase Inhibition Studies.* The potential of the synthesized triazinoindole derivatives to inhibit cholinesterases (ChEs) was assessed *in vitro* using a previously reported procedure (Ellman's method).[20] All the test compounds displayed IC_{50} values for both enzymes comparable to the parent compound (**1**) as shown in Table 1. Among them, compound **60** exhibited the highest AChE (IC_{50} value of 0.32 μM) and BuChE (IC_{50} value of 0.21 μM) inhibitory activities. Insertion of a halo substituent in the indole ring of the parent compound (**1**) showed a moderate decline in cholinesterase inhibitory activity as observed in compounds (**51−55**). Likewise, monoalkyl substituents, i.e., a methyl group at the C8 position in compound **56** and an ethyl group at the C8 position in compound **59** were also unfavorable to the ChE inhibitory activity. Insertion of dialkyl substituents, i.e., 6,9-dimethyl or 7,9-dimethyl substituents in compound **57** and compound **58**, respectively, improved the BuChE inhibitory activity. Compound **57** showed improvement in AChE and BuChE inhibitory activities (IC_{50} values of 0.41 μM and 0.23 μM, respectively). Compound **60** with a piperidine ring at the C8 position offered a significant improvement in the AChE and

https://dx.doi.org/10.1021/acschemneuro.0c00448
ACS Chem. Neurosci. XXXX, XXX, XXX−XXX

Table 1. *In Vitro h*AChE, *Eq*BuChE, Self-Mediated Aβ Aggregation Inhibitory, and Free Radical Scavenging Activities (DPPH Assay) of Compounds 51−61[f]

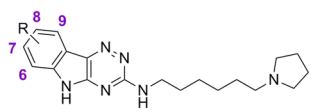

(51-60)

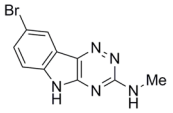

(61)

Compd	R	IC_{50} ± SEM (μM)		SI[c]	Aβ_{1-42} aggregation Inhibition (%)[d]	RP of DPPH[e] % inhibition at 20 μM
		*h*AChE[a]	*Eq*BuChE[b]			
51	8-Cl	0.98 ± 0.09	1.18 ± 0.13	1.20	40.17 ± 2.32	55.3 ± 2.4
52	6,8-diCl	1.06 ± 0.12	0.94 ± 0.07	0.89	43.84 ± 2.44	58.6 ± 2.1
53	8-Br	1.45 ± 0.23	1.14 ± 0.15	0.78	45.01 ± 1.22	55.1 ± 3.7
54	6-F	0.91 ± 0.04	1.42 ± 0.21	1.56	51.04 ± 1.15	54.3 ± 2.8
55	8-F	0.94 ± 0.03	1.53 ± 0.10	1.62	53.82 ± 2.31	52.7 ± 2.4
56	8-Me	1.16 ± 0.09	1.84 ± 0.17	1.58	57.49 ± 1.65	51.4 ± 3.3
57	6,9-diMe	0.41 ± 0.12	0.23 ± 0.08	0.56	64.25 ± 1.44	49.5 ± 2.7
58	7,9-diMe	0.54 ± 0.15	0.79 ± 0.12	1.46	58.42 ± 1.72	48.4 ± 3.2
59	8-Et	1.54 ± 0.18	1.70 ± 0.25	1.10	56.99 ± 2.58	52.6 ± 1.8
60		**0.32 ± 0.04**	**0.21 ± 0.05**	**0.65**	**54.28 ± 1.46**	**55.8 ± 2.1**
61	-	15.2 ± 0.15	8.37 ± 1.02	0.55	37.52 ± 1.31	54.7 ± 2.7
Donepezil		0.023 ± 0.01	1.87 ± 0.08	81.3	nd	> 500
Tacrine		0.056 ± 0.01	0.008 ± 0.00	0.14	nd	> 500
Ascorbic Acid		nd	nd	-	nd	13.9 ± 1.80 μM (IC_{50})
Curcumin		nd	nd	-	20.43 ± 1.05 μM (IC_{50})	nd

[a]AChE from human erythrocytes. [b]BuChE from equine serum. [c]Selectivity index = IC_{50} (BuChE)/IC_{50} (AChE). [d]Aβ_{1-42} peptide/inhibitor 1:1 with 25 μM inhibitor concentration. [e]RP of DPPH (%) = reduction percentage of DPPH. nd, not determined. [f]IC_{50} = 50% inhibitory concentration (means ± SEM of three experiments).

BuChE inhibitory activities in comparison to the parent compound (**1**). Compound **60** showed a 1.75-fold increase in AChE inhibitory activity (IC_{50} value of 0.32 μM) and a 3.2-fold increase in BuChE inhibitory activity (IC_{50} value of 0.21 μM) in comparison to compound **1**. Substituting the 6-pyrrolidinylhexyl chain in compound **60** with a small methyl group led to compound **61** which exhibited moderate ChE inhibition (AChE: IC_{50} value of 15.2 μM, BuChE: IC_{50} value of 8.37 μM), evidently proving that the basic hexyl chain is an indispensable pharmacophore for cholinesterase inhibition in this series of compounds.

3.2.2. In Vitro Antioxidant Assay. The oxidative stress induced by reactive radicals has been identified to be closely related to AD.[27] Hence, compounds that decrease the reactive radical species could confer therapeutic efficacy to AD patients. The DPPH radical scavenging assay was used to determine the antioxidant potential of the compounds as reported previously.[20] All the test compounds showed significant free radical scavenging activity ranging from 48 to 56% at 20 μM concentration (Table 1). The potent free radical scavenging activity of these derivatives resides in the electron-rich indole ring having a high resonance stability. Herein, the free −NH group of the indole ring can serve as hydrogen radical (H·) or electron donor to impart antioxidant potential to these molecules. Compound **52** exhibited significant free radical scavenging activity (58.6% at 20 μM concentration) whereas donepezil and tacrine at this concentration were observed to have relatively poor free radical scavenging activity.

3.2.3. Self-Mediated Aβ_{1-42} Aggregation Inhibition Study. The ability of the synthesized compounds to inhibit self-induced Aβ_{1-42} aggregation was evaluated using a previously detailed protocol (Thioflavin T (ThT) fluorescence assay).[20] Self-mediated Aβ_{1-42} aggregation inhibition activities of all the synthesized compounds (25 μM concentrations) are summarized in Table 1. Curcumin was used as a reference compound in this assay. All the triazinoindole derivatives exhibited significant self-induced Aβ_{1-42} aggregation inhibition ranging from 37.52 to 64.25%. Compounds (**51**−**55**) having halogen substituents on the phenyl ring of indole showed comparatively lower inhibition, whereas compounds (**56**−**59**) having alkyl substituents showed excellent Aβ_{1-42} aggregation inhibition. In this series, compound **57** exhibited the most competent Aβ_{1-42} aggregation inhibition (64.25%) at 25 μM concentration. Compound **61** with a small aminomethyl group

https://dx.doi.org/10.1021/acschemneuro.0c00448
ACS Chem. Neurosci. XXXX, XXX, XXX−XXX

at the C3 position exhibited relatively poorer Aβ_{1-42} aggregation inhibitory activity (37.52%) than compound **60** having aminohexylpyrrolidine moiety at the C3 position which evidently suggested that this basic side chain was involved in the interaction of the inhibitor with the Aβ_{1-42} peptide.

On the basis of its *in vitro* activity profile, compound **60** was selected for further evaluation, i.e., for BBB permeability study and *in vivo* animal study.

3.2.4. In Vitro Blood-Brain Barrier (BBB) Permeation Study. The BBB permeation is an essential requirement for the successful CNS active agents. The potential of the most active compound **60** to permeate across the BBB was evaluated using a parallel artificial membrane permeation assay (PAMPA) as previously reported.[20] The PAMPA assay is generally used as an indicator of a molecule's passive diffusion through the BBB. A total of seven commercial drugs having reference permeability values [P_e(ref)] were used to validate the assay. A plot of the experimental permeability values [P_e(exp)] versus the reference permeability values [P_e(ref)] offered a linear relationship, i.e., $P_e(\text{exp}) = 1.16\ P_e(\text{ref}) + 0.1668$ ($R^2 = 0.9781$) (Figure S33, Supporting Information). Considering this equation and the BBB permeation limits set by Di et al.,[28,29] it was asserted that compounds having P_e(exp) higher than 4.8 $\times 10^{-6}$ cm s^{-1} (Table S2, Supporting Information) would cross the BBB. Compound **60** displayed permeability values beyond this limit (Table 2). An experimental P_e value implied a high ability of the compounds to permeate the BBB through passive diffusion and reach the target site in CNS.

Table 2. Prediction of BBB Permeation of Compound 60 and Donepezil in the PAMPA Assay[a]

compd	P_e (10^{-6} cm s^{-1})	prediction
60	7.46 ± 2.1	CNS+
donepezil	14.3 ± 1.7	CNS+

[a]Data are expressed as mean ± SEM of three independent experiments.

3.3. Computational Studies. *3.3.1. Docking Studies of Compound 60 with ChEs.* Docking studies were performed to gain insights into the putative binding mode and molecular interactions of the most promising compound, compound **60**, in the active sites of *Tc*AChE (PDB code: 2CKM) and *h*BuChE (PDB code: 4BDS).[30]

A docking experiment of compound **60** with AChE suggested that the compound was orientated in the active site in a way similar to that of donepezil, with the Trp84 residue at the catalytical active site (CAS) to the Tyr121 residue at the peripheral anionic site (PAS). Dual binding site inhibitors demonstrating such interactions with these key amino acid residues are expected to display an excellent inhibitory activity. In a normal binding mode, a basic tricyclic ring short of any amine side chain in the structure is commonly oriented near the CAS; but in compound **60**, the binding mode is observed to be inverted wherein the planar tricyclic scaffold interacted with the PAS, and the pyrrolidine ring of compound **60** was oriented toward the CAS (Figure 2). In PAS, the tricyclic scaffold exhibited a very strong $\pi-\pi$ interaction with Tyr121 (*h*AChE: Tyr124). At physiological pH, the nitrogen of the pyrrolidine ring is protonated and showed highly stable cation-π interactions with Trp84 and Phe330 (*h*AChE: Trp86, Phe337) along with a salt bridge interaction with Glu199 (*h*AChE: Glu202) and hydrogen bonding with His440 (*h*AChE: His447).

The binding pose of **60** within the BuChE active sites is represented in Figure 3. The terminal aromatic ring of the triazinoindole scaffold exhibited $\pi-\pi$ interactions with the Phe329. The −NH of the indole ring showed hydrogen bond interaction with the Ser198 residue. The −NH group at the C3 position of the triazinoindole ring interacted by a hydrogen bond with the Glu197 residue. The protonated nitrogen of the pyrrolidine ring showed the cation-π interaction with the Asp70 residue along with a hydrogen bonding interaction with the Tyr332 residue which further provided stability to the receptor−ligand complex.

To understand the interactions between Aβ_{1-42} and compound **60**, a blind docking was performed over the entire peptide sequence using the Aβ_{1-42} monomer structure (PDB code: 1IYT).[31] Concerning Aβ aggregation, the significant residues are the hinge regions (Arg5-Ser8 and Glu22-Asn27), central hydrophobic core (Leu17-Ala21), hydrophobic region (Ile32-Ala42), and N-terminal region. In this analysis, the utmost stable peptide-ligand complex exhibited favorable interactions (Figure 4). Compound **60** was oriented along with the Aβ_{1-42} peptide. The tricyclic triazinoindole ring was observed to form stable $\pi-\pi$ interactions with the Tyr10 residue, whereas −NH of the indole ring formed a hydrogen bond with the Glu3 residue. The protonated nitrogen of pyrrolidine was observed to form a hydrogen bond and a stable

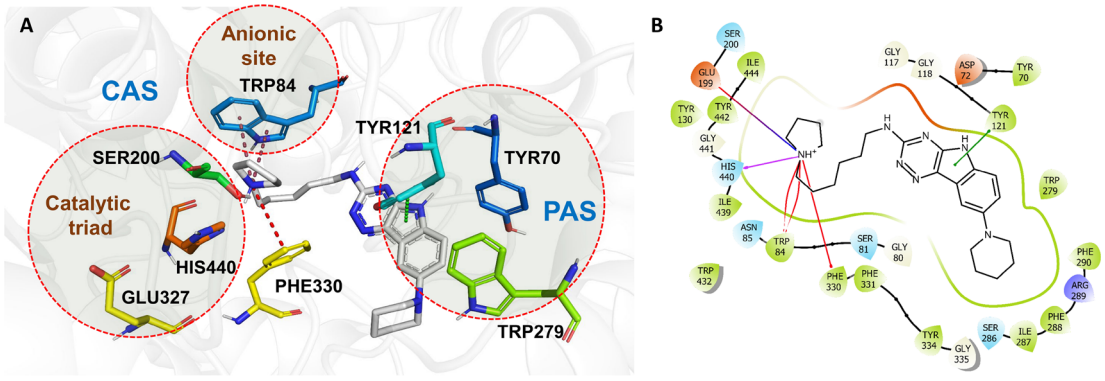

Figure 2. Molecular docking of compound **60** with *Tc*AChE (PDB ID: 2CKM). (A) Interacting pose of **60** in the active site of *Tc*AChE. The ligand is displayed as gray balls and sticks. Amino acid residues are displayed as atom type color sticks. (B) Two-dimensional representation of the interactions of **60** with the *Tc*AChE active site.

https://dx.doi.org/10.1021/acschemneuro.0c00448
ACS Chem. Neurosci. XXXX, XXX, XXX−XXX

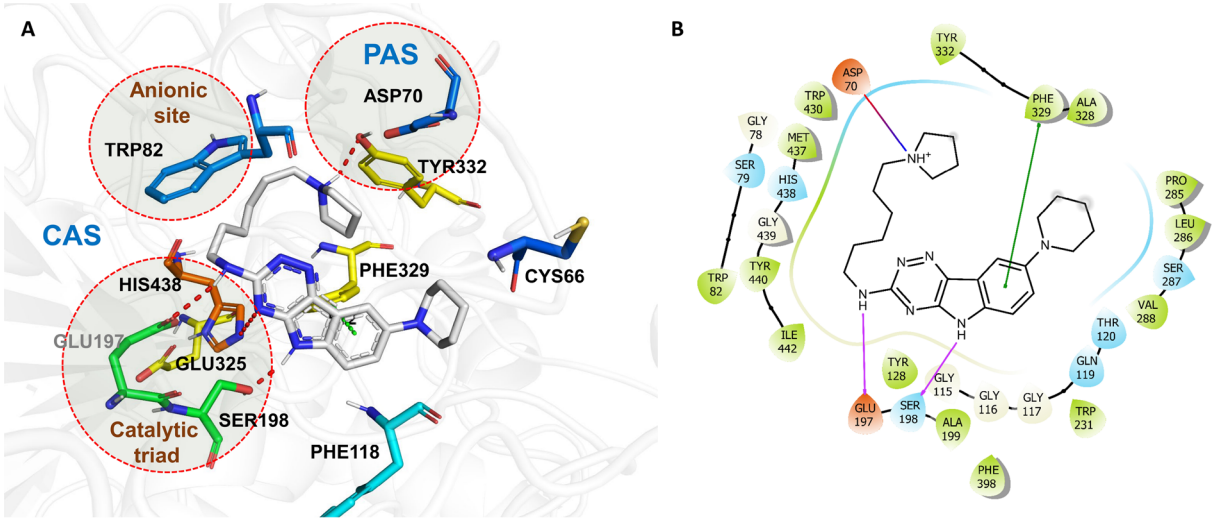

Figure 3. Molecular docking of compound **60** with *h*BuChE (PDB ID: 4BDS). (A) Interacting pose of **60** in the active site of *h*BuChE. The ligand is displayed as gray balls and sticks. Amino acid residues are displayed as atom type color sticks. (B) Two-dimensional representation of the interactions of **60** with the *h*BuChE active site.

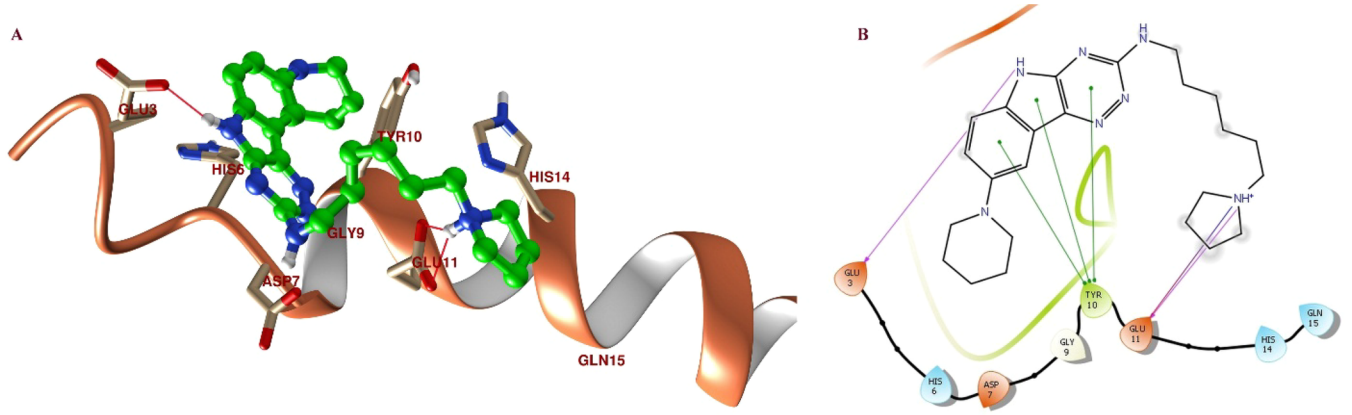

Figure 4. Molecular docking of compound **60** with the Aβ_{1-42} monomer (PDB ID: 1IYT): (A) Interaction pose of **60** with the Aβ_{1-42} monomer. The ligand is displayed as green balls and sticks. Aβ_{1-42} is displayed as a cartoon. (B) Two-dimensional representation of the interactions of **60** with Aβ_{1-42}.

salt bridge with the Glu11 residue. Mainly the hydrophobic, hydrogen bonding, and salt bridge interactions are important factors which influence the Aβ aggregation. Here, the binding of compound **60** with the Aβ_{1-42} monomer through multiple $\pi-\pi$ interactions, hydrogen bonding, and salt bridge interactions indicates that compound **60** could inhibit Aβ aggregation by suppressing intermolecular interactions of multiple Aβ monomers.

3.3.2. Molecular Dynamics Simulation Studies. The promising interactions observed between compound **60** and AChE and BuChE enzymes were validated further using time-dependent molecular dynamics stability analysis. In order to elucidate these interactions, a molecular dynamics study was carried out for a period of 20 ns by using Gromacs2020.1 and various statistical properties such as RMSD-P, RMSD-L, and RMSF-P (P = protein, L = ligand), and other intermolecular parameters like H-bonding, radius of gyration (RoG), Solvent Accessible Surface Area (SASA), etc. were examined. Using the docked pose of the receptor−ligand complex as a reference frame, all the properties were calculated.

The protein RMSD is mainly determined to know the extent of movements of receptor atoms or groups in the presence of a ligand inside the receptor active site. The analysis results revealed the structural stability, deviation, and conformations of the receptor structure over the study time period. The RMSD-P value for AChE in complexation with compound **60** was observed in a range of 0.08 to 0.18 nm with an average value of 0.14 nm (Figure 5A). This suggests that there was no major fluctuation in the receptor structure, while the ligand is in the active site and supports the stability of the system over the duration of the study. The RMSD-L for ligand fit in the receptor active site, despite having multiple rotatable bonds, was found in a range of 0.25 to 0.56 nm with an average RMSD value of 0.43 nm (Figure 5B). This strongly suggests the stability of the ligand with the receptor, and there is no change in the orientation of the ligand in the receptor active site throughout the simulation period. The residual mobility and structural integrity of the receptor were enumerated with the help of RMSF. Including the terminal residues and loop regions of the receptor, while having compound **60** in the active site, all the residues showed the RMSF-P below 0.5 nm (Figure 5C). Further, the number of hydrogen bonds between the receptor−ligand complex throughout the simulation period were determined using Gromacs g_hbond utility. A maximum

https://dx.doi.org/10.1021/acschemneuro.0c00448
ACS Chem. Neurosci. XXXX, XXX, XXX−XXX

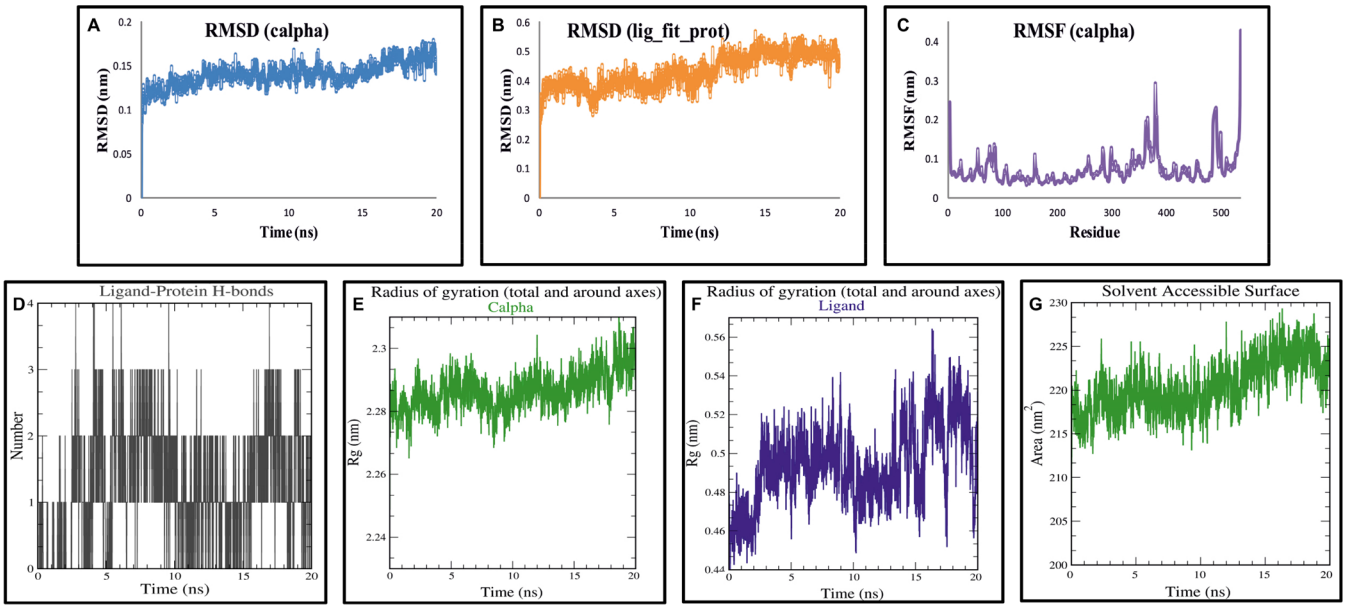

Figure 5. A. RMSD-P, B. RMSD-L, C. RMSF-P, D. H-bond, E. ROG_calpha, F. ROG_lig, and G. SASA plots for AChE with compound **60**.

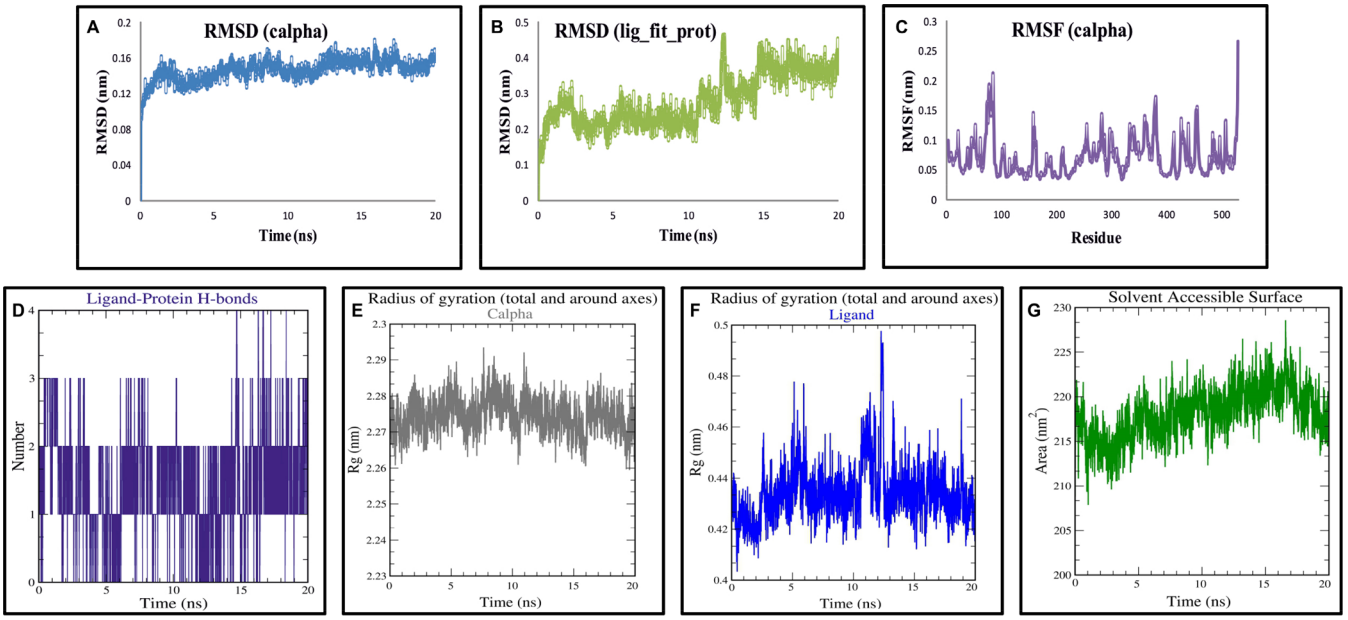

Figure 6. A. RMSD-P, B. RMSD-L, C. RMSF-P, D. H-bond, E. ROG_calpha, F. ROG_lig, and G. SASA plots for BuChE with compound **60**.

of four hydrogen bonds were observed between the ligand and the receptor, whereas two to three H-bonds were consistently present throughout the simulation period (Figure 5D). Further, SASA and radius of gyration (RoG) were observed in the range, supporting the stability of the ligand−receptor complex and the validity of the docking studies (Figures 5E−5G). Additionally, the short-range electrostatic (Coul-SR) and van der Waals/hydrophobic (LJ-SR) interaction energies between the ligand and the receptor were calculated within Gromacs. The averages of −135.28 ± 11 kJ/mol (Coul-SR) and −205.79 ± 5.9 kJ/mol (LJ-SR) were observed. High values for both of these parameters suggested that the ligand interacted promisingly strongly with the receptor active site by both electrostatic and hydrophobic interactions; wherein the role of hydrophobic interactions was observed to be higher than that of electrostatic interactions throughout the simulation period.

In a similar way, the MD study of compound **60** with BuChE was also performed. The RMSD-P value for BuChE in complexation with compound **60** was observed in a range of 0.09 to 0.18 nm with an average value of 0.15 nm (Figure 6A). This suggests that there was no major fluctuation in the receptor structure, while the ligand was in the active site and supported the stability of the system over the period of time. The RMSD-L for ligand fit in the receptor active site, despite having multiple rotatable bonds, was found in the range of 0.1 to 0.46 nm with a mean RMSD value of 0.28 nm (Figure 6B). This strongly suggests the stability of the ligand with the receptor, and there is no change in the orientation of the ligand in the receptor active site throughout the simulation period. The RMSF-P value below 0.27 nm suggests minimal local

https://dx.doi.org/10.1021/acschemneuro.0c00448
ACS Chem. Neurosci. XXXX, XXX, XXX−XXX

Table 3. Prediction of ADMET Indicators for Compound 60, Donepezil, Tacrine, and Curcumin[a]

parameter	limit	compd 60	donepezil	tacrine	curcumin
MW	130−725	421.587	379.498	198.267	368.385
HBD	0−6	2	0	1.5	2
HBA	2−20	6.5	5.5	2	7
$QPlogP_{o/w}$	−2 to 6.5	4.5	4.242	2.536	2.820
NRB	0−8	8	6	1	12
PSA	7 to 200	75.37	46.234	33.825	113.253
rule of five (violation)	0−1	0	0	0	0
volume	500−2000	1474.544	1248.451	701.299	1218.705
ReFG	0−2	0	0	0	2
SASA	300−1000	833.996	681.675	425.06	710.536
CNS	0−1	0	1	1	−2
QPMDCK		112.817	589.289	1602.036	62.279
QPlogBB	−3 to 1.2	−0.8	0.223	0.047	−2.291
QPPCaco		231.988	1070.771	2965.755	147.007
QPlogKhSa	−1.5 to 1.5	0.929	0.516	0.049	0.009
QPlogS	−6.5 to 0.5	−6.395	−4.059	−3.036	−4.653
% HOA	0−100	95.663	100	100	82.246
#star	0−5	0	0	0	0

[a]MW: molecular weight, HBD: hydrogen-bond donor atoms, HBA: hydrogen-bond acceptor atoms, $QPlogP_{o/w}$: predicted *n*-octanol/water partition coefficient, NRB: number of rotatable bonds, PSA: polar surface area, ReFG: number of reactive functional groups, SASA: total solvent accessible surface area, CNS: predicted central nervous system activity on a −2 (inactive) to +2 (active) scale, QPMDCK: predicted apparent MDCK cell permeability in nm/s, QPPCaco: caco-2 cell permeability in nm/s, QPlogBB: brain-blood partition coefficient, QPlogKhsa: binding to human serum albumin, QPlogS: predicted aqueous solubility,% HOA: human oral absorption on 0−100% scale, #star: number of parameters' values that fall outside the 95% range of similar values for known drugs.

changes in all the protein residues while having the ligand in the active site (Figure 6C).

Further, a maximum of four hydrogen bonds was observed between the ligand and the receptor, while two to three of them were consistently present throughout the simulation time (Figure 6D). Additionally, the observation of SASA and RoG values in the range supported the stability of the ligand−receptor complex and the validity of the docking studies (Figures 6E−6G). The short-range electrostatic (Coul-SR) and van der Waals/hydrophobic (LJ-SR) interaction energies between the ligand and the receptor were observed −119.17 ± 6.8 kJ/mol and −176.09 ± 3.1 kJ/mol, respectively. Both these high values suggested that the ligand interacted in a promising way with the receptor by both electrostatic and hydrophobic types of interactions, and the role of hydrophobic interactions was observed to be higher than that of the electrostatic interactions throughout the simulation period.

3.3.3. In Silico ADMET Prediction. The ADMET properties like Lipinski's parameters, PSA, $QPlogP_{o/w}$, QPlogBB, QPMDCK, QPLogKhsa, QPPCaco, etc. were predicted for the most promising compound **60** as well as for donepezil, tacrine, and curcumin using the QikProp module of Schrodinger (Table 3).[32]

Lipinski's rule of five indicates that a molecule should possess molecular weight ≤ 500, number of H-bond acceptors ≤ 10, number of H-bond donors ≤ 5, and LogP ≤ 5 for a good drugability.[33] A compound could suffer from poor oral absorption or permeation through biological membranes if it violates more than one of these parameters. Compound **60** is predicted to be a promising drug candidate as it does not infringe upon any one of the Lipinski's rule of five. Veber and co-workers introduced two other important parameters, i.e., number of rotatable bonds (NRB) and topological polar surface area (TPSA).[34] NRB is a topological parameter indicative of molecular flexibility which provides a good correlation with the oral bioavailability of drugs. Molecules having eight rotatable bonds or not more than seven atoms in linear chains outside the rings show better oral bioavailability. TPSA is another critical parameter that has shown a good correlation to passive diffusion across the membranes. It enables the prediction of drug absorption, bioavailability, and BBB permeation.[35] The marketed CNS drugs have a TPSA value in a range of 4.63−108 $Å^2$ with a mean value of 40.5 $Å^2$.[36] Compound **60** has eight rotatable bonds and a TPSA value of 75.37 $Å^2$. QPPCaco-2 is indicative of the apparent gut-blood barrier permeability. Values higher than 25 imply better oral absorption which was secured by the test compound (**60**). Likewise, the predicted human oral absorption percent (% HOA) value further supports the notable oral bioavailability of the compound. Other parameters like *n*-octanol−water partition coefficient ($QPlogP_{o/w}$), brain-blood partition coefficient (QPlogBB), apparent MDCK cell permeability (QPPMDCK), and CNS allow us to predict the potential of a compound to permeate across the BBB, which is a prerequisite for a compound to demonstrate good CNS activity. Compounds having $logP_{o/w}$ values of ∼3 showed good penetration across the BBB through passive diffusion.[37] The test ligand is predicted to have a borderline CNS penetration as it possesses a value of $QPlogP_{o/w}$ as 4.5, a value of CNS as zero, and a value of logBB as −0.8. MDCK (Madin-Darby canine kidney) cell permeability is regarded as a passable mimic for the BBB permeability.[38] The QPPMDCK value above 25 is considered as acceptable, and the test ligand possesses a significantly high value. Compound **60** showed compliance with the suggested value for QPlogKhsa, implying that the compound would possess less serum albumin binding and the free fraction of the compound would have more access to the target protein. The parameter #star indicates the number of descriptors' values that drop outside the 95% range of corresponding descriptors' values for known drugs. A large

https://dx.doi.org/10.1021/acschemneuro.0c00448
ACS Chem. Neurosci. XXXX, XXX, XXX−XXX

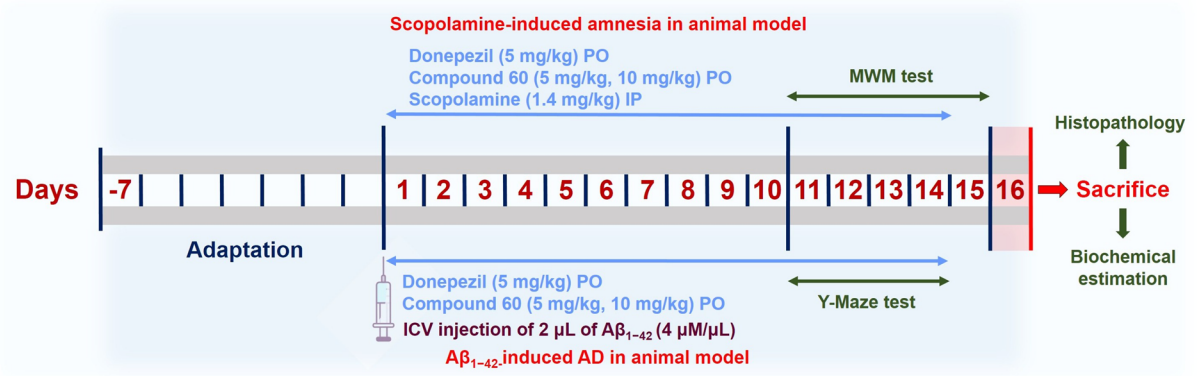

Figure 7. Schematic representation of the experimental design for evaluation of cognitive improvement in animal models of AD.

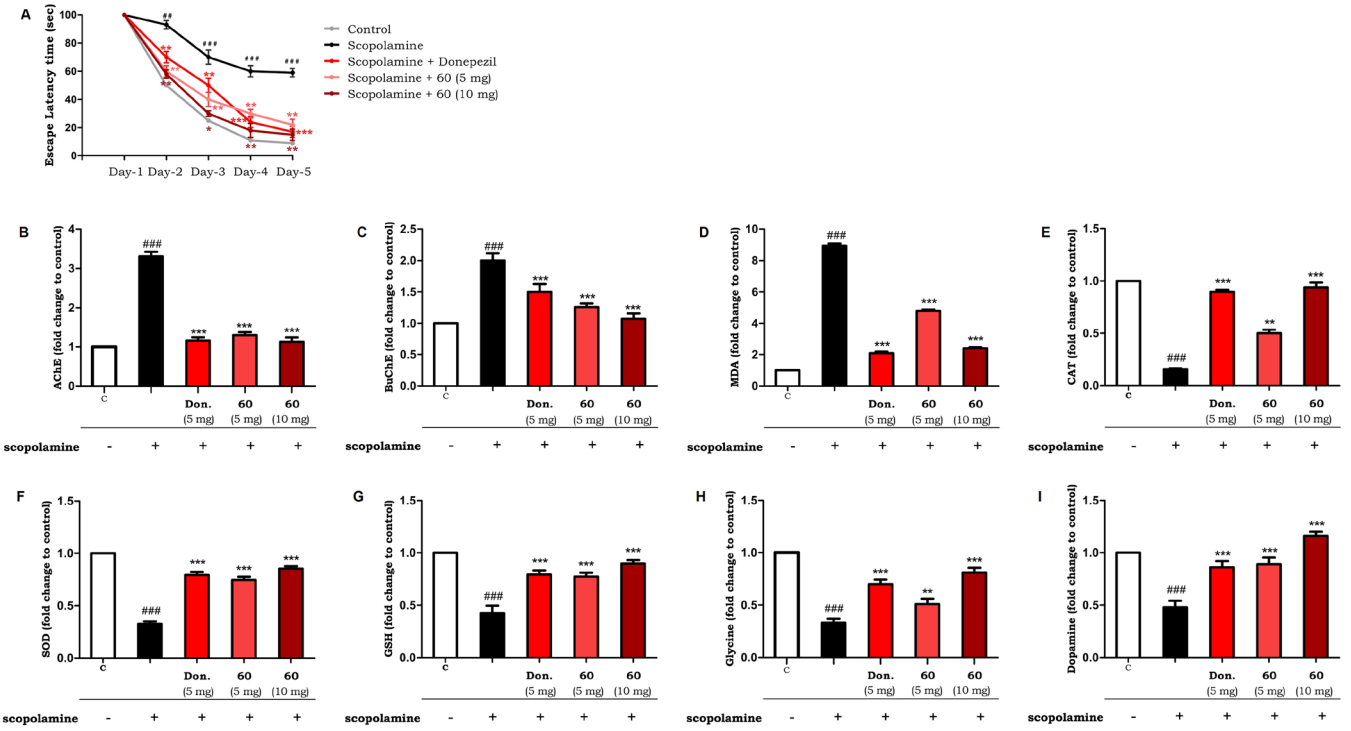

Figure 8. Anti-AD effects of compound **60** in the scopolamine-induced amnesia animal model. (**A**) MWM test; effect of compound **60** on (**B**) AChE, (**C**) BuChE, (**D**) MDA, (**E**) catalase, (**F**) SOD, (**G**) GSH, (**H**) glycine, and (**I**) dopamine levels in the brains of animals. Data are expressed as mean ± SEM (n = 7): (###) $p < 0.001$, (#) $p < 0.05$ vs the vehicle-treated control group; (***) $p < 0.001$, (**) $p < 0.01$ vs the scopolamine-treated control group. C = the vehicle-treated control group.

value of #star signifies that a ligand would be less drug-like than a ligand with a low #star value. The #star value for compound **60** indicates its drug-likeness. Furthermore, a tertiary nitrogen-containing moiety, a salient attribute present in the structure of various CNS acting agents, confers higher brain permeation.[36] Thus, it can be predicted that compound **60** would have a favorable pharmacokinetic profile which further magnifies its biological importance.

3.4. Assessment of Cognitive Improvement in an Animal Model of AD. Based on the results of the *in vitro* studies of the synthesized triazinoindole derivatives, compound **60** was chosen for further *in vivo* assessment of its anti-AD potential. To assess the effect of **60** on the improvement of cognitive functions, scopolamine-induced amnesia and Aβ_{1-42}-induced AD animal models were used. The brief experimental design is depicted in Figure 7.

3.4.1. Morris Water Maze Test. Scopolamine-induced amnesia in rodents was used as an animal model to evaluate the potential of **60** on memory improvement.[20] The Morris water maze (MWM) test was performed to evaluate the hippocampal-dependent spatial learning ability of the animals. To assess the reference or long-term memory, the escape latency time (ELT) was monitored during the last 5 days of the treatment period. Scopolamine (1.4 mg/kg, IP) treatment significantly prolonged the ELT (Figure 8A). ELT was considerably shortened in the donepezil- (5 mg/kg, PO) treated group compared to that of the scopolamine-treated control group. Compound **60** (5 mg/kg and 10 mg/kg, PO) significantly shortened the ELT in comparison to the scopolamine-treated control group. These observations showed that the animals could retain the preceding memory

https://dx.doi.org/10.1021/acschemneuro.0c00448
ACS Chem. Neurosci. XXXX, XXX, XXX−XXX

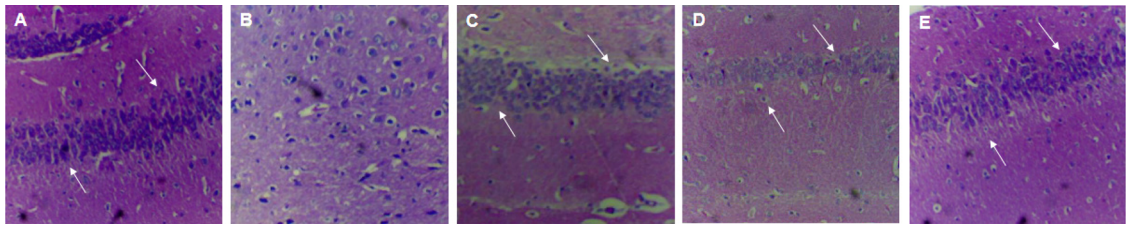

Figure 9. Hematoxylin and eosin staining of the pyramidal cells in the hippocampal region: (**A**) normal control, (**B**) scopolamine-treated, (**C**) donepezil-treated, (**D**) test compound-treated (5 mg/kg), and (**E**) test compound-treated (10 mg/kg) animals' brains. The white arrows indicate pyramidal cells in the hippocampal region.

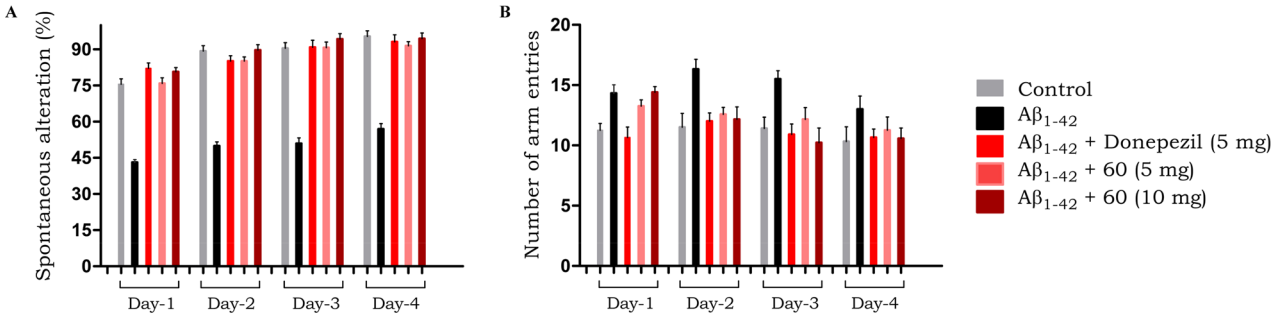

Figure 10. Y-maze test to assess the immediate working memory in Aβ_{1-42}-treated rats. (**A**) Percentage of spontaneous alterations and (**B**) number of arm entries. Data are expressed as mean ± SEM (n = 7).

in the Morris water maze test, reflecting the spatial memory improvement.

3.4.2. Neurochemical Analysis and Histology. The effect of compound **60** on ChEs levels, oxidant stress parameters, and level of neurotransmitters in the brain was evaluated after MWM test completion. The cholinesterase level in the brain was considerably elevated in animals by scopolamine treatment. The effect of compound **60** on the cholinesterase level was evaluated using Ellman's method. The increased levels of ChEs (Figures 8B and 8C) were reduced notably by the treatment of compound **60**.

Malondialdehyde (MDA), catalase, superoxide dismutase (SOD), and glutathione (GSH) levels in the brain were also estimated further to ascertain the *in vivo* antioxidant activity of compound **60** as shown in Figure 8.[39,40] Quantitative assessment of the lipid peroxidation products in the brain homogenate is estimated by the thiobarbituric acid reactive substances (TBARS) assay as reported previously.[20] The MDA level was raised in the scopolamine-treated group (Figure 8D) as compared to the vehicle-treated control group. Compound **60** treatment to the amnesic mice significantly diminished the rise in MDA levels (Figure 8D) in comparison to the scopolamine-treated group. With biochemical assessment of the catalase, an antioxidant enzyme is carried out which provides the amount of the hydrogen peroxide breakdown. The catalase level was significantly reduced in scopolamine-treated animals with respect to the vehicle-treated control group animals. However, administration of the compound **60** to the amnesic mice significantly increased the catalase level (Figure 8E). SOD is an antioxidant enzyme, which plays an important role in neutralizing superoxide anions. Scopolamine administration notably reduced SOD levels in the brains of treated animals in comparison to the control group (Figure 8F). However, compound **60** treatment to the amnesic mice markedly increased the SOD levels (Figure 8F). Glutathione (GSH) is an antioxidant tripeptide molecule synthesized in the cytoplasm and available in higher concentrations in the mitochondria. It protects cells from oxidative damage by neutralizing free radicals. The glutathione level declines with an increase in oxidative stress. It is noticeable that scopolamine-treated animals showed a significant reduction in GSH levels (Figure 8G) compared to the control group animals. Administration of **60** to the amnesic mice increased GSH levels (Figure 8G). These results confirmed the *in vivo* antioxidant potential of the test compound (**60**).

It is reported that the levels of glycine and dopamine in the brain also decline in dementia.[41−43] Therefore, their levels in the brain were estimated to support the anti-AD potential of compound **60**. Scopolamine administration markedly reduced glycine levels in the brains of treated animals in comparison to the control group (Figure 8H). Administration of compound **60** to the amnesic mice notably increased glycine levels (Figure 8H) in comparison to the scopolamine-treated group. The augmented levels of glycine could ameliorate the NMDA receptor hypofunction which helps in the improvement of the cognitive function. Further, the scopolamine-treated group exhibited reduced levels of dopamine (Figure 8I) in the brain as compared to the control group. Treatment with compound **60** increased the dopamine levels as compared to the scopolamine-treated group (Figure 8I). Compound **60** at the dose of 5 mg/kg restored the dopamine level to normal, whereas at the dose of 10 mg/kg, it showed an increase in the dopamine level as compared to the normal group.

After executing the MWM test, the histopathological study of the brain was carried out to evaluate the effect of compound **60** on pyramidal cells in the hippocampal region in the scopolamine-induced amnesic animals' brains.[44] Hematoxylin-eosin staining of the hippocampus of the normal control animal showed regular four to five layers of pyramidal cells with a prominent nucleus and uniform morphology (Figure 9A). In qualitative analysis of pyramidal cells, the scopolamine-treated group showed impairment in pyramidal cells in

https://dx.doi.org/10.1021/acschemneuro.0c00448
ACS Chem. Neurosci. XXXX, XXX, XXX−XXX

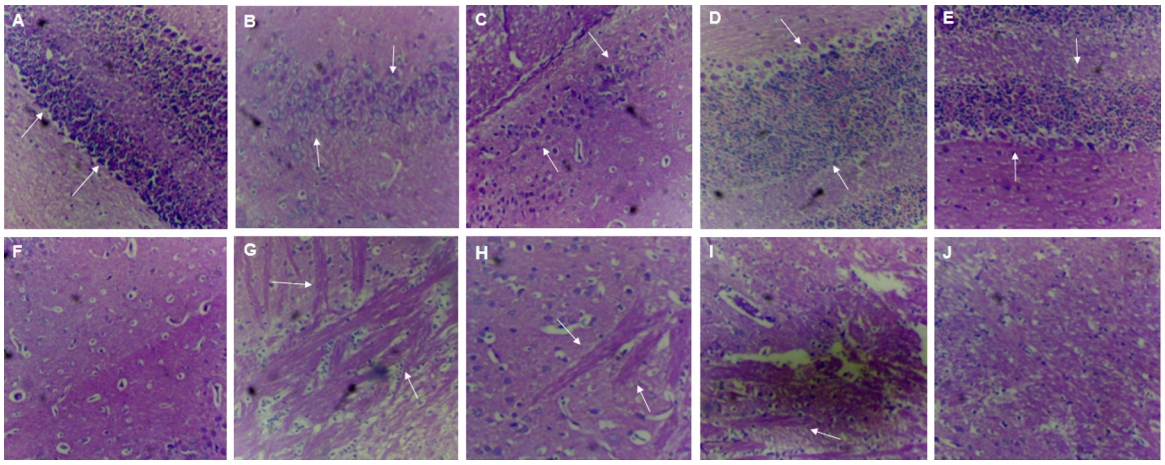

Figure 11. Effect of compound **60** on pyramidal cells and Aβ fibrils formation in the hippocampal region of Aβ_{1-42}-treated animals' brains: (**A**, **F**) vehicle-treated control, (**B**, **G**) Aβ-treated, (**C**, **H**) donepezil-treated, (**D**, **I**) test compound-treated (5 mg/kg), and (**E**, **J**) test compound-treated (10 mg/kg) animals' brains. The white arrows indicate pyramidal cells and Aβ fibrils.

comparison to the normal control group as the number of pyramidal cells were reduced, and the layers were obscured with disordered cell arrangement (Figure 9B). The donepezil-treated group showed layers of organized pyramidal cells (Figure 9C). Treatment of the amnesic mice with compound **60** offered protection to the pyramidal cells (Figures 9D and 9E) as an ordered arrangement of layers of pyramidal cells was observed in the compound **60**-treated group. It could be concluded from the observations that compound **60** treatment restores the neuronal structure and protects the neurons from scopolamine-induced damage.

3.4.3. Y-Maze Test. The Aβ_{1-42}-induced AD animal model was adopted to evaluate the effect of compound **60** on cognitive functions.[20] Aβ_{1-42} was injected intracerebroventricularly (ICV) in the hippocampal region of the brain, and working memory impairment was assessed using the Y-maze test. The short-term or spatial working memory was evaluated as spontaneous alterations in the behavior of the animals. Aβ_{1-42} injected in rats significantly lowered the spontaneous alternations as compared to the normal vehicle treatment. Donepezil treatment significantly increased spontaneous alternations in comparison to the Aβ_{1-42}-treated group. Treatment of animals with test compound **60** (dose: 5 mg/kg and 10 mg/kg) remarkably reversed Aβ_{1-42}-induced alleviation in spontaneous alternations (Figure 10A). The general locomotor activity was not affected by the treatment of compound **60** as the mean value for the number of arm entries remains steady for all the animal groups (Figure 10B). Thus, the treatment of animals with compound **60** improved Aβ_{1-42}-impaired hippocampal-dependent working memory.

After completion of the Y-maze test, the histopathological study of the brain was carried out to evaluate the protective effect of compound **60** on pyramidal cells in the hippocampal region and Aβ fibril formation in the brain.[44] Hematoxylin-eosin staining of the hippocampus of the vehicle-treated control animal showed regular four to five layers of pyramidal cells with a prominent nucleus and uniform morphology (Figure 11A). In qualitative analysis of pyramidal cells, the Aβ_{1-42}-treated group showed impairment in pyramidal cells. The pyramidal cells were reduced in number and became scattered, and the layers became obscured (Figure 11B). The donepezil-treated group showed organized pyramidal cells' layers (Figure 11C). Treatment of the animals with compound **60** offered protection to the pyramidal cells against the neurotoxicity induced by Aβ_{1-42} (Figures 11D and 11E). Layers of compact pyramidal cells having ordered cell arrangement were observed in the compound **60**-treated group. The histopathological study showed formation of Aβ fibrils in the brains of the control group animals (Figure 11G). In qualitative analysis of Aβ fibrils, treatment with donepezil and compound **60** (5 mg/kg) in Aβ_{1-42}-treated rats offered reduction in Aβ fibrils (Figures 11H and 11I). A few or negligible number of Aβ fibrils could be observed in rats having compound **60** (10 mg/kg) treatment (Figure 11J). Hence, the results suggested that compound **60** provided neuronal protection against the Aβ_{1-42}-induced toxicity and reduced the Aβ fibril formation in brains of Aβ_{1-42}-treated animals.

Results obtained from the behavioral studies, neurochemical and oxidative stress parameters, and histopathological observations in the scopolamine-induced amnesia model as well as the Aβ_{1-42}-induced AD model showed that compound **60** has the potential to reverse the working and reference memory deficit, protect the pyramidal cells against stress-induced damage, diminish the Aβ fibril formation, and control the oxidative stress-induced dementia.

3.4.4. Acute Toxicity Study. Acute toxicity of the most promising compound, compound **60**, was accessed as per the OECD 423 guidelines using Wistar female rats as discussed in the previous report.[20] After oral administration of compound **60** (dose: 2000 mg/kg, n = 3 per group), the animals were monitored continuously for any abnormal behavior and mortality during the first 4 h. Afterward, the animals were periodically monitored for the next 14 days for any sign of delayed effects. All the animals managed to survive the span of the study period and appeared stable in terms of fur sleekness, water and food consumption, and body weight. All the animals were sacrificed on the 15th day, and the organs like heart, lungs, kidneys, and liver were macroscopically examined for any damage. There were no apparent changes noticed in these organs. The observations from this study pointed out that compound **60** treatment to the rats did not show any acute toxicity or mortality immediately or throughout the post-treatment period. Hence, compound **60** can be viewed as nontoxic and well-tolerated at doses up to 2000 mg/kg.

https://dx.doi.org/10.1021/acschemneuro.0c00448
ACS Chem. Neurosci. XXXX, XXX, XXX−XXX

4. CONCLUSION

Considering the multifactorial nature of Alzheimer's disease, attempts have been made to further explore some novel derivatives of the previously reported triazinoindole scaffold for exploring their anti-AD potential. A novel series of substituted triazinoindole derivatives were rationally designed, synthesized, and assessed for their multitarget directed anti-AD activities. In this series, compound **60** having a piperidine ring at the C8 position of the triazinoindole scaffold was identified as the most potent cholinesterase inhibitor with IC_{50} values of 0.32 μM and 0.21 μM for AChE and BuChE, respectively. Compound **60** exhibited remarkable self-mediated $A\beta_{1-42}$ aggregation inhibition (54% at 25 μM concentration). These derivatives exhibited excellent free radical scavenging activity. Molecular modeling studies demonstrated prominent interactions by the most promising compound **60** with ChEs as well as with the $A\beta_{1-42}$ peptide. Compound **60** displayed reasonably good permeability in the PAMPA-BBB assay. Considering the impressive *in vitro* profile of compound **60**, it was chosen for *in vivo* assessment of its anti-AD potential in rodent models. Compound **60** successfully reversed the memory deficit in both MWM and Y-Maze tests. MDA, catalase, SOD, and GSH levels were restored to around their normal values asserting the antioxidant potential of compound **60**. The histopathological study of the brain implies that compound **60** provides protection to the pyramidal cells against neuronal toxicity and reduces Aβ fibril formation in the amnesic animals. Additionally, compound **60** is endowed with the ability to restore the glycine and dopamine levels nearly close to their normal values in scopolamine-treated animals. It remained nontoxic with the administration of a single highest dose of 2000 mg/kg in rats. Compound **60** exhibited promising virtual ADMET properties. Altogether, these results highlight the potential of compound **60** as a prospective lead to develop novel MTDLs as anti-AD drug.

5. EXPERIMENTAL SECTION

5.1. General. All chemicals required for the synthesis of the final compounds were purchased from Spectrochem and used as received. Progress of the reaction was observed by thin-layer chromatography (TLC) (silica gel 60 F_{254} precoated aluminum plates) and visualized in UV light (λ = 254 nm) or an iodine chamber. For the purification of the final compounds, flash column chromatography (Teledyne ISCO CombiFlash Rf system) was used. The purity of the final compounds was checked by HPLC. All the compounds displayed not less than a 95% purity level. The HPLC method is detailed in the Supporting Information. Melting points were determined in open capillary tubes using the Veego melting point apparatus and are uncorrected. The IR spectra in KBr pellets were recorded on an FT-IR spectrophotometer for all the synthesized compounds and are accordant with their respective structures. ^{1}H NMR spectra were obtained in the DMSO-d_6 solvent at 400 MHz on a Bruker Advance-II spectrometer. Chemical shift values (δ) were reported in parts per million (ppm) with respect to tetramethylsilane (TMS) as internal standard. Peak patterns were described as singlet (s), doublet (d), triplet (t), multiplet (m), and broad signal (br). Mass spectra were obtained on a Thermo Fisher mass spectrometer using an electrospray ion source. Elemental analyses were carried out by a Thermo Fisher FLASH 2000 organic elemental analyzer and showed the elemental compositions of the compounds were within ±0.4% of the calculated values. All the animal studies reported here were performed by following CPCSEA guidelines and regulations and were reviewed and endorsed by the institutional animal ethics committee (IAEC) (Approval No. MSU/IAEC/2018-19/1803).

5.2. Chemistry. *5.2.1. Synthesis of Substituted Isatins (11−20).* Substituted isatins (**11−19**) were synthesized by the two-step Sandmeyer isatin synthetic process (**Method A**).[25]

Method A: Step 1. Sodium sulfate (6 equiv) and chloral hydrate (1 equiv) were dissolved in water (100 mL) in a round-bottomed flask. Substituted aniline (**2−10**, 5.0 g, 1 equiv) dissolved in concentrated HCl (40 mL) was added to the mixture, and the mixture was stirred vigorously for 30 min at room temperature. Hydroxylamine HCl (3 equiv) solution in water (10 mL) was added to the reaction mixture. The resultant mixture was heated to 70 °C for 6−8 h. Once the reaction was completed (monitored by TLC), ice-cold water was added to the reaction mixture. The precipitates of α-isonitrosoacetanilide so obtained were filtered, washed with water, dried, and used in the next step without further purification.

Step 2. To a round-bottomed flask charged with concentrated sulfuric acid (10 mL) and water (1 mL) was added α-isonitrosoacetanilide (1.0 g) over a period of a few minutes. The resulting deep red solution was heated to 80 °C for 4 h and then cooled to room temperature. The reaction mixture was added to a vigorously stirred mixture of ice water (100 mL) and ethyl acetate (50 mL). The organic phase was separated, and the aqueous phase was extracted with ethyl acetate (50 mL × 2). The combined red organic phase was dried over anhydrous magnesium sulfate, filtered, and evaporated under reduced pressure to obtain the titled compound.

5.2.1a. 5-Chloroisatin (11). The title compound (**11**) was synthesized from 4-chloroaniline (**2**, 5.0 g, 39.19 mmol) following **Method A**. Dark orange solid (yield: 4.41 g, 62%); mp 245−247 °C (lit.[45] mp 244−245 °C); IR (KBr, cm^{-1}): 3324, 3130, 3062, 2933, 2853, 1637, 1582, 1557; MS (m/z): 182.02 [M + H]$^+$.

5.2.1b. 5,7-Dichloroisatin (12). The title compound (**12**) was synthesized from 2,4-dichloroaniline (**3**, 5.0 g, 30.86 mmol) following **Method A**. Reddish yellow solid (yield: 3.45 g, 52%); mp 221−223 °C (lit.[46] mp 228−230 °C); IR (KBr, cm^{-1}): 3068, 1751, 1704, 1615, 1309, 846, 747; MS (m/z): 217 [M + H]$^+$.

5.2.1c. 5-Bromoisatin (13). The title compound (**13**) was synthesized from 4-bromoaniline (**4**, 5.0 g, 29.07 mmol) following **Method A**. Orange solid (yield: 4.1 g, 62%); mp 247−249 °C (lit.[46] mp 248−250 °C); IR (KBr, cm^{-1}): 3454, 3180, 3104, 1743, 1613, 1318, 688; MS (m/z): 224 [M − 2]$^+$.

5.2.1d. 7-Fluoroisatin (14). The title compound (**14**) was synthesized from 2-fluoroaniline (**5**, 5.0 g, 44.97 mmol) following **Method A**. Yellowish orange solid (yield: 3.86 g, 52%); mp 192−194 °C (lit.[47] mp 186−190 °C); IR (KBr, cm^{-1}): 3169, 3031, 1736, 1638, 1260, 1037; MS (m/z): 166 [M + H]$^+$.

5.2.1e. 5-Fluoroisatin (15). The title compound (**15**) was synthesized from 4-fluoroaniline (**6**, 5.0 g, 44.97 mmol) following **Method A**. Dark red colored solid (yield: 4.30 g, 58%); mp 226−228 °C (lit.[47] mp 223−225 °C); IR (KBr, cm^{-1}): 3095, 1753, 1705, 1616, 1309; MS (m/z): 166.04 [M + H]$^+$.

5.2.1f. 5-Methylisatin (16). The title compound (**16**) was synthesized from 4-methylaniline (**7**, 5.0 g, 46.66 mmol) following **Method A**. Reddish brown solid (yield: 4.89 g, 65%); mp 184−187 °C (lit.[48] mp 183−184 °C); IR (KBr, cm^{-1}): 3288, 1749, 1704, 1625, 1301, 828, 737; MS (m/z): 162.16 [M + H]$^+$.

5.2.1g. 4,7-Dimethylisatin (17). The title compound (**17**) was synthesized from 2,5-dimethylaniline (**8**, 5.0 g, 41.26 mmol) following **Method A**. Red solid (yield: 3.04 g, 42%); mp 190−192 °C; IR (KBr, cm^{-1}): 3207, 3107, 1730, 1594, 1320, 957, 809, 712; MS (m/z): 176.09 [M + H]$^+$.

5.2.1h. 4,6-Dimethylisatin (18). The title compound (**18**) was synthesized from 3,5-dimethylaniline (**9**, 5.0 g, 41.26 mmol) following **Method A**. Red solid (yield: 3.25 g, 45%); mp 228−231 °C (lit.[49] mp 239−241 °C); IR (KBr, cm^{-1}): 3201, 1756, 1722, 1626, 1269, 747; MS (m/z): 176.06 [M + H]$^+$.

5.2.1i. 5-Ethylisatin (19). The title compound (**19**) was synthesized from 4-ethylaniline (**10**, 5.0 g, 41.26 mmol) following **Method A**. Red solid (yield: 3.90 g, 53%); mp 131−133 °C; IR (KBr, cm^{-1}): 3284, 1746, 1709, 1619, 1488, 1317, 694; MS (m/z): 176.05 [M + H]$^+$.

https://dx.doi.org/10.1021/acschemneuro.0c00448
ACS Chem. Neurosci. XXXX, XXX, XXX−XXX

*5.2.1j. 5-(Piperidin-1-yl)isatin (**20**).* To a solution of piperidine (0.44 mL, 4.24 mmol) in DMF (10 mL) were added potassium carbonate (0.74 g, 5.31 mmol) and 5-bromoisatin (**13**, 1.0 g, 4.24 mmol). The reaction mixture was allowed to stir at 60 °C for 6−8 h until the completion of the reaction (monitored by TLC). Once the reaction was completed, the reaction mixture was poured into crushed ice. The precipitated product so formed was collected by filtration, washed with water, and dried to get the red colored title compound (**20**). (Yield: 0.57 g, 56%); mp 150−152 °C (lit.[26] mp 154−156 °C); IR (KBr, cm^{-1}): 3419, 2938, 1623, 1541, 1240, 825, 748; MS (m/z): 231 $[M + H]^+$.

*5.2.2. Synthesis of Substituted 5H-[1,2,4]triazino[5,6-b]indol-3-thiol Derivatives (**21**−**30**).* **Method B:** To a suspension of substituted isatins (**11**−**19**, 1.0 g, 1 equiv) in aqueous potassium carbonate solution (1 equiv in 50 mL of water) was added thiosemicarbazide (1 equiv). The resultant mixture was refluxed for 11−15 h. A clear liquid was obtained by hot filtration of reaction mixture. Once the liquid was cooled down to room temperature, the solution was acidified with glacial acetic acid and left for 3−5 h. The precipitate so obtained was filtered and washed with dilute acetic acid (5%). The obtained solid was triturated with hot DMF, filtered, and dried to yield the titled compound as a yellow solid.[20,50]

*5.2.2a. 8-Chloro-5H-[1,2,4]triazino[5,6-b]indole-3-thiol (**21**).* The title compound (**21**) was synthesized from 5-chloroisatin (**11**, 1.0 g, 5.51 mmol) and thiosemicarbazide (0.50 g, 5.51 mmol) as per **Method B**. Yellow solid (yield: 0.99 g, 76%); mp >250 °C; IR (KBr, cm^{-1}): 3095, 2992, 1617, 1458, 1310, 1166, 847; MS (m/z): 237 $[M + H]^+$.

*5.2.2b. 6,8-Dichloro-5H-[1,2,4]triazino[5,6-b]indole-3-thiol (**22**).* The title compound (**22**) was synthesized from 5,7-dichloroisatin (**12**, 1.0 g, 4.63 mmol) and thiosemicarbazide (0.42 g, 4.63 mmol) as per **Method B**. Light yellow solid (yield: 0.85 g, 68%); mp >250 °C; IR (KBr, cm^{-1}): 3289, 3061, 1605, 1433, 1318, 1146, 841; MS (m/z): 271 $[M]^+$, 273 $[M + 2]^+$.

*5.2.2c. 8-Bromo-5H-[1,2,4]triazino[5,6-b]indole-3-thiol (**23**).* The title compound (**23**) was synthesized from 5-bromoisatin (**13**, 1.0 g, 4.42 mmol) and thiosemicarbazide (0.40 g, 4.42 mmol) as per **Method B**. Yellow solid (yield: 0.95 g, 76%); mp >250 °C (lit.[50] mp >250 °C); IR (KBr, cm^{-1}): 3359, 3091, 1600, 1449, 1313, 1167, 813; MS (m/z): 281 $[M]^+$.

*5.2.2d. 6-Fluoro-5H-[1,2,4]triazino[5,6-b]indole-3-thiol (**24**).* The title compound (**24**) was synthesized from 7-fluoroisatin (**14**, 1.0 g, 6.06 mmol) and thiosemicarbazide (0.55 g, 6.06 mmol) as per **Method B**. Yellow solid (yield: 0.92 g, 69%); mp >250 °C; IR (KBr, cm^{-1}): 3424, 3063, 1621, 1480, 1320, 1141, 1015; MS (m/z): 221 $[M + H]^+$.

*5.2.2e. 8-Fluoro-5H-[1,2,4]triazino[5,6-b]indole-3-thiol (**25**).* The title compound (**25**) was synthesized from 5-fluoroisatin (**15**, 1.0 g, 6.06 mmol) and thiosemicarbazide (0.55 g, 6.06 mmol) as per **Method B**. Yellow solid (yield: 0.96 g, 72%), mp >250 °C. IR (KBr, cm^{-1}): 3425, 3014, 1620, 1477, 1320, 1140, 1015; MS (m/z): 221 $[M + H]^+$.

*5.2.2f. 8-Methyl-5H-[1,2,4]triazino[5,6-b]indole-3-thiol (**26**).* The title compound (**26**) was synthesized from 5-methylisatin (**16**, 1.0 g, 6.2 mmol) and thiosemicarbazide (0.56 g, 6.2 mmol) as per **Method B**. Yellow solid (yield: 1.1 g, 82%); mp >250 °C; IR (KBr, cm^{-1}): 3438, 3030, 2884, 1609, 1477, 1323, 1190, 1142; MS (m/z): 217 $[M + H]^+$.

*5.2.2g. 6,9-Dimethyl-5H-[1,2,4]triazino[5,6-b]indole-3-thiol (**27**).* The title compound (**27**) was synthesized from 4,7-dimethylisatin (**17**, 1.0 g, 6.2 mmol) and thiosemicarbazide (0.52 g, 5.71 mmol) as per **Method B**. Yellow solid (yield: 0.89 g, 68%); mp >250 °C; IR (KBr, cm^{-1}): 3391, 3034, 2935, 1586, 1439, 1325, 1149; MS (m/z): 231 $[M + H]^+$.

*5.2.2h. 7,9-Dimethyl-5H-[1,2,4]triazino[5,6-b]indole-3-thiol (**28**).* The title compound (**28**) was synthesized from 4,6-dimethylisatin (**18**, 1.0 g, 6.2 mmol) and thiosemicarbazide (0.52 g, 5.71 mmol) as per **Method B**. Yellow solid (yield: 0.82 g, 63%); mp >250 °C; IR (KBr, cm^{-1}): 3021, 2871, 1611, 1432, 1303, 1163; MS (m/z): 231 $[M + H]^+$.

*5.2.2i. 8-Ethyl-5H-[1,2,4]triazino[5,6-b]indole-3-thiol (**29**).* The title compound (**29**) was synthesized from 5-ethylisatin (**19**, 1.0 g, 5.71 mmol) and thiosemicarbazide (0.52 g, 5.71 mmol) as per **Method B**. Yellow solid (yield: 0.84 g, 68%), mp >250 °C; IR (KBr, cm^{-1}): 3433, 3029, 2877, 1604, 1478, 1320, 1186, 1141; MS (m/z): 231 $[M + H]^+$.

*5.2.2j. 8-(Piperidin-1-yl)-5H-[1,2,4]triazino[5,6-b]indole-3-thiol (**30**).* The title compound (**30**) was synthesized from 5-(piperidin-1-yl)isatin (**20**, 1.0 g, 4.34 mmol) and thiosemicarbazide (0.40 g, 4.34 mmol) as per **Method B**. Yellow solid (yield: 0.83 g, 67%); mp >250 °C; IR (KBr, cm^{-1}): 3361, 3089, 1599, 1449, 1312, 1239, 1167; MS (m/z): 286 $[M + H]^+$.

*5.2.3. Synthesis of Substituted 3-(Methylthio)-5H-[1,2,4]triazino-[5,6-b]indole Derivatives (**31**−**40**).* **Method C:** To a stirring suspension of substituted 5*H*-[1,2,4]-triazino[5,6-*b*]indole-3-thiol derivatives (**21**−**30**, 1.0 g, 1 equiv) in dimethylformamide (15 mL) was added potassium carbonate (1 equiv) followed by methyl iodide (1 equiv). The reaction mixture was stirred at room temperature for 6−8 h until completion (monitored by TLC). Once the reaction was completed, the reaction mixture was poured into ice water. The obtained solid was collected filtration, washed with water, and dried to yield the titled compounds (**31**−**40**).[20]

*5.2.3a. 8-Chloro-3-(methylthio)-5H-[1,2,4]triazino[5,6-b]indole (**31**).* The title compound (**31**) was synthesized from **21** (1.0 g, 4.22 mmol) and methyl iodide (0.26 mL, 4.22 mmol) according to **Method C**. Greenish yellow solid (yield: 0.82 g, 77%); mp >250 °C. IR (KBr, cm^{-1}): 3446, 3048, 2933, 1606, 1454, 1186, 825, 780; MS (m/z): 251 $[M]^+$, 253 $[M + 2]^+$.

*5.2.3b. 6,8-Dichloro-3-(methylthio)-5H-[1,2,4]triazino[5,6-b]-indole (**32**).* The title compound (**32**) was synthesized from **22** (1.0 g, 4.22 mmol) and methyl iodide (0.23 mL, 3.69 mmol) according to **Method C**. Greenish yellow solid (yield: 0.75 g, 71%); mp >250 °C; IR (KBr, cm^{-1}): 3047, 2962, 2860, 1606, 1452, 1183, 820, 775; MS (m/z): 285 $[M]^+$, 287 $[M + 2]^+$.

*5.2.3c. 8-Bromo-3-(methylthio)-5H-[1,2,4]triazino[5,6-b]indole (**33**).* The title compound (**33**) was synthesized from **23** (1.0 g, 3.56 mmol) and methyl iodide (0.23 mL, 3.56 mmol) following **Method C**. Light yellow solid (yield: 0.77 g, 73%); mp >250 °C; IR (KBr, cm^{-1}): 3047, 2961, 1607, 1316, 1183, 1091, 820, 776; MS (m/z): 295 $[M]^+$, 297 $[M + 2]^+$.

*5.2.3d. 6-Fluoro-3-(methylthio)-5H-[1,2,4]triazino[5,6-b]indole (**34**).* The title compound (**34**) was synthesized from **24** (1.0 g, 3.56 mmol) and methyl iodide (0.28 mL, 4.54 mmol) according to **Method C**. Light yellow solid (yield: 0.73 g, 68%); mp >250 °C; IR (KBr, cm^{-1}): 3106, 3054, 2955, 1611, 1495, 1321, 1155; MS (m/z): 235 $[M + H]^+$.

*5.2.3e. 8-Fluoro-3-(methylthio)-5H-[1,2,4]triazino[5,6-b]indole (**35**).* The title compound (**35**) was synthesized from **25** (1.0 g, 3.56 mmol) and methyl iodide (0.28 mL, 4.54 mmol) according to **Method C**. Light yellow solid (yield: 0.76 g, 72%); mp >250 °C; IR (KBr, cm^{-1}): 3054, 2954, 1609, 1323, 1156, 820; MS (m/z): 235 $[M + H]^+$.

*5.2.3f. 8-Methyl-3-(methylthio)-5H-[1,2,4]triazino[5,6-b]indole (**36**).* The title compound (**36**) was synthesized from **26** (1.0 g, 4.62 mmol) and methyl iodide (0.29 mL, 4.62 mmol) according to **Method C**. Light yellow solid (yield: 0.70 g, 66%); mp >250 °C; IR (KBr, cm^{-1}): 3061, 2976, 1603, 1471, 1319, 1208, 977, 814; MS (m/z): 231 $[M + H]^+$.

*5.2.3g. 6,9-Dimethyl-3-(methylthio)-5H-[1,2,4]triazino[5,6-b]-indole (**37**).* The title compound (**37**) was synthesized from **27** (1.0 g, 4.34 mmol) and methyl iodide (0.27 mL, 4.34 mmol) according to **Method C**. Light yellow solid (yield: 0.79 g, 75%); mp 212−214 °C; IR (KBr, cm^{-1}): 3093, 2965, 2920, 1588, 1334, 1180, 809, 752; MS (m/z): 245 $[M + H]^+$.

*5.2.3h. 7,9-Dimethyl-3-(methylthio)-5H-[1,2,4]triazino[5,6-b]-indole (**38**).* The title compound (**38**) was synthesized from **28** (1.0 g, 4.34 mmol) and methyl iodide (0.27 mL, 4.34 mmol) according to **Method C**. Light yellow solid (yield: 0.77 g, 73%); mp >250 °C; IR (KBr, cm^{-1}): 3049, 2966, 2919, 1589, 1426, 1313, 1179, 844, 752; MS (m/z): 245 $[M + H]^+$.

https://dx.doi.org/10.1021/acschemneuro.0c00448
ACS Chem. Neurosci. XXXX, XXX, XXX−XXX

*5.2.3i. 8-Ethyl-3-(methylthio)-5H-[1,2,4]triazino[5,6-b]indole (**39**).* The title compound (**39**) was synthesized from **29** (1.0 g, 4.34 mmol) and methyl iodide (0.27 mL, 4.34 mmol) according to **Method C**. Light yellow solid (yield: 0.73 g, 69%); mp >250 °C; IR (KBr, cm^{-1}): 3062, 2961, 1599, 1480, 1318, 1204, 972, 806, 739; MS (m/z): 245 $[M + H]^+$.

*5.2.3j. 3-(Methylthio)-8-(piperidin-1-yl)-5H-[1,2,4]triazino[5,6-b]-indole (**40**).* The title compound (**40**) was synthesized from **30** (1.0 g, 3.5 mmol) and methyl iodide (0.22 mL, 3.5 mmol) according to **Method C**. Light yellow solid (yield: 0.71 g, 67%); mp >250 °C; IR (KBr, cm^{-1}): 3087, 2966, 1607, 1453, 1317, 1183, 1092, 976, 819, 778; MS (m/z): 300 $[M + H]^+$.

*5.2.4. Synthesis of Substituted 3-(Methylsulfonyl)-5H-[1,2,4]-triazino[5,6-b]indole Derivatives (**41**–**50**).* To a stirred solution of substituted 3-(methylthio)-5*H*-[1,2,4]triazino[5,6-*b*]indoles (**31**–**40**, 1.0 g, 1 equiv) in anhydrous methylene chloride (20 mL) at 0–5 °C was gradually added *m*-CPBA (2.25 equiv) in small portions over a period of 5 min. The resultant reaction mixture was stirred at room temperature maintaining anhydrous conditions for 24 h. Once the reaction was completed (monitored by TLC), the reaction mixture was washed repeatedly with a sodium bicarbonate solution (5%) and with brine. The obtained organic phase was dried over anhydrous magnesium sulfate, filtered, and concentrated under reduced pressure to obtain a light greenish-yellow solid. The obtained products were used as such in the next step without further purification.[20]

*5.2.5. Synthesis of Substituted N-(Aminoalkyl)-5H-[1,2,4]-triazino[5,6-b]indol-3-amine Derivatives (**51**–**61**).* **Method D:** To substituted 3-(methylsulfonyl)-5*H*-[1,2,4]triazino[5,6-*b*]indoles (**41**–**50**, 0.5 g, 1 equiv) in tetrahydrofuran (15 mL) was added 6-(pyrrolidin-1-yl)hexan-1-amine or methyl amine (5 equiv). The reaction mixture was heated to reflux until the completion of the reaction (monitored by TLC). Once the reaction was completed, the reaction mixture was diluted with ice cold water (50 mL) and extracted with ethyl acetate (30 mL × 3). The combined organic phase was washed with a sodium bicarbonate solution (5%) and then with brine, dried over anhydrous sodium sulfate, and concentrated under reduced pressure. The crude material so obtained was further purified by flash chromatography.[20]

*5.2.5a. 8-Chloro-N-(6-(pyrrolidin-1-yl)hexyl)-5H-[1,2,4]triazino-[5,6-b] indol-3-amine (**51**).* The title compound (**51**) was synthesized from sulfone (**41**, 0.5 g, 1.77 mmol) and 6-(pyrrolidin-1-yl)hexan-1-amine (3.01 g, 17.7 mmol) as per **Method D**. Yellow solid (yield: 0.46 g, 70%); mp >250 °C; IR (KBr, cm^{-1}): 3421, 3075, 2930, 1618, 1547, 1365, 1142, 1107, 816; ^{1}H NMR (DMSO-d_6): δ 11.84 (bs, 1H, −N*H*), 8.02 (d, J = 2.2 Hz, 1H, Ar*H*), 7.43 (dd, J = 8.5, 2.2 Hz, 1H, Ar*H*), 7.36 (d, J = 8.5 Hz, 1H, Ar*H*), 3.34–3.42 (m, 2H, −NHCH_2), 2.42–2.54 (m, 6H, −NCH_2), 1.59–1.71 (m, 4H, −NCH$_2$CH_2), 1.52–1.57 (m, 2H, −NCH$_2$CH_2), 1.39–1.45 (m, 2H, −NHCH$_2$CH_2), 1.25–1.34 (m, 4H, −CH_2); MS (m/z): 373 $[M]^+$, 375 $[M + 2]^+$; RP-HPLC: purity = 96.7%, t_R = 4.08 min.

*5.2.5b. 6,8-Dichloro-N-(6-(pyrrolidin-1-yl)hexyl)-5H-[1,2,4]-triazino[5,6-b]indol-3-amine (**52**).* The title compound (**52**) was synthesized from sulfone (**42**, 0.5 g, 1.58 mmol) and 6-(pyrrolidin-1-yl)hexan-1-amine (2.69 g, 15.8 mmol) as per **Method D**. Yellow solid (yield: 0.44 g, 68%); mp >250 °C; IR (KBr, cm^{-1}): 3405, 3062, 2931, 1608, 1528, 1376, 1312, 1076, 834, 724; ^{1}H NMR (DMSO-d_6): δ 7.43 (d, J = 2.1 Hz, 1H, Ar*H*), 7.39 (d, J = 2.1 Hz, 1H, Ar*H*), 3.35–3.45 (m, 2H, −NHCH_2), 2.36–2.51 (m, 6H, −NCH_2), 1.56–1.71 (m, 6H, −NCH$_2$CH_2), 1.42–1.49 (m, 2H, −NHCH$_2$CH_2), 1.31–1.40 (m, 4H, −CH_2); MS (m/z): 407.31 $[M]^+$, 409.25 $[M + 2]^+$; RP-HPLC: purity = 97.6%, t_R = 6.88 min.

*5.2.5c. 8-Bromo-N-(6-(pyrrolidin-1-yl)hexyl)-5H-[1,2,4]triazino-[5,6-b] indol-3-amine (**53**).* The title compound (**53**) was synthesized from sulfone (**43**, 0.5 g, 1.53 mmol) and 6-(pyrrolidin-1-yl)hexan-1-amine (2.61 g, 15.3 mmol) as per **Method D**. Yellow solid (yield: 0.41 g, 64%); mp >250 °C; IR (KBr, cm^{-1}): 3415, 3073, 2929, 1615, 1524, 1453, 1142, 1106, 738; ^{1}H NMR (DMSO-d_6): δ 8.18 (d, J = 2.0 Hz, 1H, Ar*H*), 7.58 (dd, J = 8.5, 2.0 Hz, 1H, Ar*H*), 7.34 (d, J = 8.5 Hz, 1H, Ar*H*), 3.35–3.40 (m, 2H, −NHCH_2), 2.30–2.38 (m, 6H, −NCH_2), 1.55–1.66 (m, 6H, −NCH$_2$CH_2), 1.28–1.46 (m, 2H, −NHCH$_2$CH_2, 4H, −CH_2); MS (m/z): 417.31 $[M]^+$, 419.09 $[M + 2]^+$; RP-HPLC: purity = 99.1%, t_R = 4.78 min.

*5.2.5d. 6-Fluoro-N-(6-(pyrrolidin-1-yl)hexyl)-5H-[1,2,4]triazino-[5,6-b] indol-3-amine (**54**).* The title compound (**54**) was synthesized from sulfone (**44**, 0.5 g, 1.88 mmol) and 6-(pyrrolidin-1-yl)hexan-1-amine (3.20 g, 18.8 mmol) as per **Method D**. Yellow solid (yield: 0.42 g, 61%); mp 221–220 °C; IR (KBr, cm^{-1}): 3235, 3108, 2935, 1584, 1526, 1361, 1128, 1026; ^{1}H NMR (DMSO-d_6): δ 11.82 (bs, 1H, −N*H*), 7.82–7.87 (m, 1H, Ar*H*), 7.34–7.41 (m, 1H, Ar*H*), 7.25–7.33 (m, 1H, Ar*H*), 3.32–3.37 (m, 2H, −NHCH_2), 2.30–2.38 (m, 6H, −NCH_2), 1.55–1.67 (m, 6H, −NCH$_2$CH_2), 1.26–1.46 (m, 2H, −NHCH$_2$CH_2, 4H, −CH_2); MS (m/z): 356 $[M]^+$, 358 $[M + 2]^+$; RP-HPLC: purity = 98.5%, t_R = 3.62 min.

*5.2.5e. 8-Fluoro-N-(6-(pyrrolidin-1-yl)hexyl)-5H-[1,2,4]triazino-[5,6-b] indol-3-amine (**55**).* The title compound (**55**) was synthesized from sulfone (**45**, 0.5 g, 1.88 mmol) and 6-(pyrrolidin-1-yl)hexan-1-amine (3.20 g, 18.8 mmol) as per **Method D**. Yellow solid (yield: 0.42 g, 63%); mp 242–245 °C; IR (KBr, cm^{-1}): 3233, 3106, 2935, 1528, 1360, 1293, 1128, 1025, 798, 735; ^{1}H NMR (DMSO-d_6): δ 11.87 (bs, 1H, −N*H*), 7.83–7.86 (m, 1H, Ar*H*), 7.36–7.39 (m, 1H, Ar*H*), 7.26–7.31 (m, 1H, Ar*H*), 3.34–3.36 (m, 2H, −NHCH_2), 2.28–2.41 (m, 6H, −NCH_2), 1.53–1.67 (m, 6H, −NCH$_2$CH_2), 1.25–1.46 (m, 2H, −NHCH$_2$CH_2, 4H, −CH_2); MS (m/z): 356 $[M]^+$, 358 $[M + 2]^+$; RP-HPLC: purity = 98.4%, t_R = 3.65 min.

*5.2.5f. 8-Methyl-N-(6-(pyrrolidin-1-yl)hexyl)-5H-[1,2,4]triazino-[5,6-b]indol-3-amine (**56**).* The title compound (**56**) was synthesized from sulfone (**46**, 0.5 g, 1.91 mmol) and 6-(pyrrolidin-1-yl)hexan-1-amine (3.25 g, 19.1 mmol) as per **Method D**. Yellow solid (yield: 0.49 g, 73%); mp 178–181 °C; IR (KBr, cm^{-1}): 3225, 3104, 2931, 1613, 1523, 1282, 1209, 1100, 801, 737; ^{1}H NMR (DMSO-d_6): δ 11.61 (bs, 1H, −N*H*), 7.80–7.91 (m, 1H, Ar*H*), 7.15–7.36 (m, 2H, Ar*H*), 3.29–3.40 (m, 2H, −NHCH_2), 2.43 (s, 3H, ArCH_3), 2.30–2.41 (m, 6H, −NCH_2), 1.54–1.74 (m, 6H, −NCH$_2$CH_2), 1.10–1.49 (m, 2H, −NHCH$_2$CH_2, 4H, −CH_2); MS (m/z): 352.93 $[M]^+$; RP-HPLC: purity = 98.7%, t_R = 3.81 min.

*5.2.5g. 6,9-Dimethyl-N-(6-(pyrrolidin-1-yl)hexyl)-5H-[1,2,4]-triazino[5,6-b]indol-3-amine (**57**).* The title compound (**57**) was synthesized from sulfone (**47**, 0.5 g, 1.81 mmol) and 6-(pyrrolidin-1-yl)hexan-1-amine (3.08 g, 18.1 mmol) as per **Method D**. Yellow solid (yield: 0.46 g, 69%); mp 154–156 °C; IR (KBr, cm^{-1}): 3228, 3010, 2930, 1599, 1518, 1264, 1121, 1032, 799, 751; ^{1}H NMR (DMSO-d_6): δ 11.44 (bs, 1H, −N*H*), 7.14 (d, J = 7.5 Hz, 1H, Ar*H*), 6.95 (d, J = 7.5 Hz, 1H, Ar*H*), 3.32–3.34 (m, 2H, −NHCH_2), 2.77 (s, 3H, ArCH_3), 2.41 (s, 3H, ArCH_3), 2.29–2.38 (m, 6H, −NCH_2), 1.56–1.66 (m, 6H, −NCH$_2$CH_2), 1.26–1.46 (m, 2H, −NHCH$_2$CH_2, 4H, −CH_2); MS (m/z): 366.94 $[M]^+$; RP-HPLC: purity = 97.5%, t_R = 4.05 min.

*5.2.5h. 7,9-Dimethyl-N-(6-(pyrrolidin-1-yl)hexyl)-5H-[1,2,4]-triazino[5,6-b]indol-3-amine (**58**).* The title compound (**58**) was synthesized from sulfone (**48**, 0.5 g, 1.81 mmol) and 6-(pyrrolidin-1-yl)hexan-1-amine (3.08 g, 18.1 mmol) as per **Method D**. Yellow solid (yield: 0.41 g, 62%); mp 168–170 °C; IR (KBr, cm^{-1}): 3372, 2931, 1619, 1312, 1136, 841, 769; ^{1}H NMR (DMSO-d_6): δ 11.72 (bs, 1H, −N*H*), 7.00 (s, 1H, Ar*H*), 6.90 (s, 1H, Ar*H*), 3.36–3.40 (m, 2H, −NHCH_2), 2.78 (s, 3H, ArCH_3), 2.37–2.49 (m, 6H, −NCH_2, 3H, ArCH_3), 1.55–1.71 (m, 6H, −NCH_2), 1.42–1.49 (m, 2H, −NHCH$_2$CH_2); 1.30–1.40 (m, 4H, −CH_2); MS (m/z): 367 $[M + H]^+$; RP-HPLC: purity = 98.9%, t_R = 4.06 min.

*5.2.5i. 8-Ethyl-N-(6-(pyrrolidin-1-yl)hexyl)-5H-[1,2,4]triazino[5,6-b] indol-3-amine (**59**).* The title compound (**59**) was synthesized from sulfone (**49**, 0.5 g, 1.81 mmol) and 6-(pyrrolidin-1-yl)hexan-1-amine (3.08 g, 18.1 mmol) as per **Method D**. Yellow solid (yield: 0.49 g, 74%); mp 167–169 °C; IR (KBr, cm^{-1}): 3226, 3012, 2933, 1613, 1525, 1379, 1100, 877, 742; ^{1}H NMR (DMSO-d_6): δ 13.21 (bs, 1H, −N*H*), 8.31 (d, J = 2.1 Hz, 1H, Ar*H*), 7.71 (dd, J = 2.1 Hz, 8.4 Hz, 1H, Ar*H*), 7.64 (d, J = 8.4 Hz, 1H, Ar*H*), 3.36–3.37 (m, 2H, −NHCH_2), 2.82–2.87 (m, 2H, ArCH_2CH$_3$), 2.31–2.38 (m, 6H, −NCH_2), 1.54–1.66 (m, 6H, −NCH$_2$CH_2), 1.28–1.44 (m, 2H,

https://dx.doi.org/10.1021/acschemneuro.0c00448
ACS Chem. Neurosci. XXXX, XXX, XXX–XXX

−NHCH$_2$CH$_2$, 4H, −CH$_2$, 3H, Ar−CH$_2$CH$_3$); MS (m/z): 367 [M + H]$^+$; RP-HPLC: purity = 97.0%, t_R = 4.38 min.

*5.2.5j. 8-(Piperidin-1-yl)-N-(6-(pyrrolidin-1-yl)hexyl)-5H-[1,2,4]-triazino[5,6-b]indol-3-amine (**60**).* The title compound (**60**) was synthesized from sulfone (**50**, 0.5 g, 1.51 mmol) and 6-(pyrrolidin-1-yl)hexan-1-amine (2.57 g, 15.1 mmol) as per **Method D**. Yellow solid (yield: 0.85 g, 67%); mp 237−241 °C; IR (KBr, cm^{-1}): 3416, 2930, 1617, 1538, 1363, 1143, 1107, 813, 737; ^{1}H NMR (DMSO-d_6): δ 11.98 (bs, 1H, −NH), 8.18 (d, J = 2.1 Hz, 1H, ArH), 7.58 (dd, J = 8.5, 2.1 Hz, 1H, ArH), 7.34 (d, J = 2.1 Hz, 1H, ArH), 3.10−3.53 (m, 2H, −NHCH$_2$, 4H, −NCH$_2$), 2.27−2.40 (m, 6H, −NCH$_2$), 1.50−1.66 (m, 6H, −NCH$_2$CH$_2$), 1.25−1.48 (m, 2H, −NHCH$_2$CH$_2$, 4H, −CH$_2$, 6H, −NCH$_2$CH$_3$, 6H,−NCH$_2$CH$_2$CH$_2$); MS (m/z): 422 [M + H]$^+$; RP-HPLC: purity = 98.9%, t_R = 4.827 min.

*5.2.5k. 8-Bromo-N-methyl-5H-[1,2,4]triazino[5,6-b]indol-3-amine (**61**).* The title compound (**61**) was synthesized from sulfone (**43**, 0.5 g, 1.53 mmol) and methylamine (2.0 M in THF, 7.72 mL, 15.3 mmol) as per **Method D**. Yellow solid (yield: 0.26 g, 61%); mp >250 °C; IR (KBr, cm^{-1}): 3426, 3076, 2972, 1632, 1552, 1193, 1048, 866, 786; ^{1}H NMR (DMSO-d_6): δ 8.16 (d, J = 2.0 Hz, 1H, ArH), 7.56 (dd, J = 8.5, 2.0 Hz, 1H, ArH), 7.33 (d, J = 8.5 Hz, 1H, ArH), 2.87 (s, 3H, −NHCH$_3$); MS (m/z): 278 [M]$^+$, 280 [M + 2]$^+$.

5.3. Biology. *5.3.1. In Vitro Cholinesterase Inhibition Assay.* The ability of the synthesized compounds to inhibit ChEs was evaluated using Ellman's method as presented in our earlier reports.[20,51,52] Tacrine and donepezil were used as standard compounds.

5.3.2. In Vitro Antioxidant Assay. The compounds' antioxidant potential was determined according to the DPPH assay as detailed in earlier reports.[20,52] Ascorbic acid was utilized as the standard antioxidant.

5.3.3. Self-Induced Aβ_{1-42} Aggregation Inhibition Study. The ability of the substituted triazinoindoles to inhibit self-mediated Aβ_{1-42} aggregation was assessed using the Thioflavin T (ThT)-based fluorescence assay as detailed in our earlier report.[52] Curcumin was used as a reference compound.

5.3.4. In Vitro Blood-Brain Barrier Permeation Study. The BBB permeability of the most promising compound, compound **60**, was predicted by the PAMPA assay as detailed in our earlier report.[20] Seven commercially available drugs having known BBB permeability data were used in the experiment to validate the protocol (Table S1, Supporting Information). A graph of the P_e(exp) versus P_e(ref) values gave a good linear correlation, P_e(exp) = 1.16 P_e(ref) + 0.1668 (R^2 = 0.9781) (Figure S33, Supporting Information).

5.3.5. Assessment of Cognitive Improvement in an AD Animal Model. 5.3.5a. Morris Water Maze Test. The Morris water maze test was performed as per the previously reported method to evaluate the spatial learning memory in the scopolamine-induced amnesia animal model.[20,53] Male adult Swiss Albino mice were used for this study.

5.3.5b. Neurochemical Analysis. Once the MWM test was completed, the animals were euthanized, and their whole brains were removed and homogenized in sodium phosphate buffer (12.5 mM, pH = 7). The homogenates were centrifuged for 15 min at 15,000 rpm and 4 °C. The resultant supernatants were used for the assessment of various biomarkers/parameters.

The cholinergic biomarkers (ChEs) and oxidative stress parameters (MDA, catalase) in the mice brains were estimated as per our previously reported methods.[20,54]

SOD activity was measured according to the method described by Misra and Frodvich.[20,55] Briefly, the tissue homogenate (0.5 mL) was diluted with double distilled water (0.5 mL), ice-cold ethanol (0.25 mL), and chloroform (0.15 mL) and mixed well for 5 min. The resulting solution was centrifuged at 2500 rpm at 4 °C for 10 min. The resulting supernatant (0.5 mL) was mixed with carbonate buffer (0.05 M, 1.5 mL) and EDTA solution (0.49 mM, 0.5 mL). Finally, the absorbance at 480 nm was measured immediately after the addition of the epinephrine solution (3 mM, 0.4 mL). The standard graph was obtained by processing the different concentrations (10−125 units) of standard SOD as described above.

GSH was estimated according to the method described by Moron et al.[56] In brief, the supernatant (0.75 mL) was added into the trichloroacetic acid solution (20%, 0.75 mL). The resulting mixture was centrifuged at 6,000 rpm for 15 min at 5−7 °C. The resulting supernatant (0.25 mL) was mixed with the DTNB solution (0.6 mM, 2 mL), and the final volume was adjusted to 3 mL with phosphate buffer (0.2 M, pH = 8.0). A blank was prepared by following the same procedure without adding a supernatant solution. The absorbance of the final solution was measured at 412 nm. The standard graph was obtained by processing the different concentrations (10−50 μg/mL) of standard GSH as described above.

The neurotransmitters' levels (glycine and dopamine) in the mice brains were estimated as per our previously reported methods.[20,57]

5.3.5c. Histopathology. After behavioral analysis, animals were euthanized, and their brains were isolated and used for the assessments of histological changes and Aβ fibril formation. Samples were fixed in 10% paraformaldehyde and then embedded in paraffin after standard processing of dehydration and clearing, and then, the brains were sectioned with 2 μm thickness in a rotary microtome, mounted on glass slides, and stained with hematoxylin and eosin for histopathological examinations.[58]

5.3.5d. Y-Maze Test. The Y-Maze test was performed as per the previously reported method to evaluate the short-term or spatial working memory in the Aβ_{1-42}-induced AD animal model.[20,59] Male adult Wistar rats were used for this study.

5.3.5e. Acute Toxicity Study. The assessment of the acute toxicity of compound **60** was carried out in Wistar female rats (200−250 g body weight) according to OECD 423 guidelines as discussed in our previous report.[20,60]

5.4. Computational Studies. *5.4.1. Docking Studies of Compound **60** with ChEs.* Docking studies of compound **60** with ChEs were performed according to the previously reported protocol using 3D crystal structures of AChE (PDB IDs: 1B41, 2CKM) and of BuChE (PDB ID: 4BDS). A Glide module (Schrodinger Suite) was used for the docking studies.[61−63]

*5.4.2. Docking Studies of Compound **60** with Aβ_{1-42}.* Docking studies of compound **60** with Aβ_{1-42} were performed according to the previously reported protocol using 3D crystallographic structures of the Aβ_{1-42} peptide (PDB ID: 1IYT). The docking study was performed using the docking program AutoDock4.2.[64,65]

5.4.3. Molecular Dynamics Simulation Studies. To study the ligand−receptor interaction consistency and stability over a period of time, molecular dynamics simulation was carried out between compound **60** and AChE and BuChE enzyme structures by using GROMACS 2020.1 software.[66] The ligand−receptor complex obtained from the docking study was taken as the initiating point for simulation. To establish the complex stability, the CHARMM36 all-atom force field was implemented, and ligand−receptor parameters were calculated in GROMACS.[67] To do so, the ligand topology was prepared and retrieved using the CGenFF server,[68,69] and the ligand−receptor complex was generated. These complexes were solvated using the TIP3P/SPC216 water model.[70] To neutralize the total charge on the individual system, Na$^+$ or Cl$^-$ ions were added to the system. Both the complexes were initially energy minimized with the steepest descent method[71] followed by two sequential equilibration simulations using canonical (NVT) and isobaric-isothermic (NPT) ensembles for 100 ps (ps) each. Taking the NPT ensemble, the final production MD simulation was carried out, and the long-range electrostatic interactions were identified by using the particle mesh Ewald (PME) method.[72] The molecular dynamics simulation study was performed for a 10 ns time period at 300 K temperature and 1 bar pressure using the GROMACS 2020.1 simulation package, and the resulting data was analyzed.[73,74]

5.4.4. In Silico Prediction of ADMET Parameters. *In silico* prediction of ADMET parameters was carried out using the QikProp module of the Schrodinger Suite.[32] The structures of the ligand molecules generated for the docking studies were used to predict various physicochemical and pharmacokinetic parameters. The key parameters that were predicted in this study were Lipinski's rule of five, polar surface area, the number of rotatable bonds, central nervous system permeability, brain/blood partition coefficient, aqueous

https://dx.doi.org/10.1021/acschemneuro.0c00448
ACS Chem. Neurosci. XXXX, XXX, XXX−XXX

solubility, apparent MDCK cell permeability, human serum albumin binding, Caco-2 cell permeability, and percent human-oral absorption.

■ ASSOCIATED CONTENT

Supporting Information

The Supporting Information is available free of charge at https://pubs.acs.org/doi/10.1021/acschemneuro.0c00448.

HPLC method, spectral data of the synthesized compounds and *in vitro* blood-brain barrier permeation assay data (PDF)

■ AUTHOR INFORMATION

Corresponding Author

Mange Ram Yadav − *Faculty of Pharmacy, Kalabhavan Campus, The Maharaja Sayajirao University of Baroda, Vadodara 390001, Gujarat, India; Director (R & D), Centre of Research for Development, Parul University, Vadodara 391760, Gujarat, India;* orcid.org/0000-0003-2020-5225; Email: mryadav11@yahoo.co.in

Authors

Dushyant V. Patel − *Faculty of Pharmacy, Kalabhavan Campus, The Maharaja Sayajirao University of Baroda, Vadodara 390001, Gujarat, India;* orcid.org/0000-0003-2984-3805

Nirav R. Patel − *Faculty of Pharmacy, Kalabhavan Campus, The Maharaja Sayajirao University of Baroda, Vadodara 390001, Gujarat, India*

Ashish M. Kanhed − *Shobhaben Pratapbhai Patel - School of Pharmacy & Technology Management, SVKM's NMIMS University, Vile Parle, Mumbai 400056, India*

Divya M. Teli − *Department of Pharmaceutical Chemistry, L. M. College of Pharmacy, Ahmedabad 380009, Gujarat, India*

Kishan B. Patel − *Faculty of Pharmacy, Kalabhavan Campus, The Maharaja Sayajirao University of Baroda, Vadodara 390001, Gujarat, India*

Pallav M. Gandhi − *Faculty of Pharmacy, Kalabhavan Campus, The Maharaja Sayajirao University of Baroda, Vadodara 390001, Gujarat, India*

Sagar P. Patel − *Faculty of Pharmacy, Kalabhavan Campus, The Maharaja Sayajirao University of Baroda, Vadodara 390001, Gujarat, India*

Bharat N. Chaudhary − *Faculty of Pharmacy, Kalabhavan Campus, The Maharaja Sayajirao University of Baroda, Vadodara 390001, Gujarat, India*

Dharti B. Shah − *Faculty of Pharmacy, Kalabhavan Campus, The Maharaja Sayajirao University of Baroda, Vadodara 390001, Gujarat, India*

Navnit K. Prajapati − *Faculty of Pharmacy, Kalabhavan Campus, The Maharaja Sayajirao University of Baroda, Vadodara 390001, Gujarat, India*

Kirti V. Patel − *Faculty of Pharmacy, Kalabhavan Campus, The Maharaja Sayajirao University of Baroda, Vadodara 390001, Gujarat, India*

Complete contact information is available at: https://pubs.acs.org/10.1021/acschemneuro.0c00448

Author Contributions

M.R.Y. conceptualized, supervised, and coordinated the whole study. D.V.P. and N.R.P. carried out the synthetic work and collected data. A.M.K. designed and carried out computational studies. D.M.T., K.B.P., and D.B.S. contributed reagents and assisted in the synthetic work and data collection. K.V.P. drafted the biological studies. P.M.G., S.P.P., and B.N.C. performed biological evaluation and data collection. N.K.P. assisted in the synthesis and data interpretation. D.V.P., N.R.P., and A.M.K. drafted the manuscript. All authors read and approved the final version of the manuscript.

Notes

The authors declare no competing financial interest.

■ ACKNOWLEDGMENTS

D.V.P. cordially acknowledges the DST-INSPIRE, New Delhi for awarding a Research Fellowship (IF-150660). N.R.P. is thankful to the UGC, New Delhi, for awarding a Senior Research Fellowship [F. No. 25-1/2014-15(BSR)/7-129/2007/(BSR)]. The authors are thankful to Dr. Amisha Vora, SPPSPTM, NMIMS University, Mumbai, for mass spectra facility support and Dr. Kapil Juvale, SPPSPTM, NMIMS University, Mumbai, for providing a SpectramMax iD3 multimode microplate reader to perform the Aβ_{1-42} aggregation study. The authors thank Bharat Senta for his generous help during the PAMPA assay and HPLC analysis of final compounds.

■ ABBREVIATIONS

AChE acetylcholinesterase
AD Alzheimer's disease
APP amyloid precursor protein
Aβ β-amyloid
BBB blood-brain barrier
BuChE butyrylcholinesterase
CAS catalytical active site
ChE cholinesterase
ELT escape latency time
XP extra precision
GSH glutathione
ICV intracerebroventricular
MDA malondialdehyde
MDCK Madin-Darby canine kidney
MWM Morris water maze
MTDLs multitarget-directed ligands
NMDA *N*-methyl-D-aspartate
PAMPA parallel artificial membrane permeation assay
PAS peripheral anionic site
PBL porcine brain lipid
RNS reactive nitrogen species
RoG radius of gyration
ROS reactive oxygen species
RMSD root-mean-square deviation
SASA solvent accessible surface area
SOM sites of metabolism
SOD superoxide dismutase
TLC thin-layer chromatography
TBARS thiobarbituric acid reactive substances
ThT Thioflavin T
TPSA topological polar surface area

■ REFERENCES

(1) Goedert, M., and Spillantini, M. G. (2006) A century of Alzheimer's disease. *Science 314*, 777−781.

(2) Alzheimer's Disease International. (2019, April 10). World Alzheimer report 2019: Attitudes to dementia. https://www.alz.co.uk/research/world-report-2019 (accessed 2020-03-08).

(3) Talesa, V. N. (2001) Acetylcholinesterase in Alzheimer's disease. *Mech. Ageing Dev. 122* (16), 1961−1969.
(4) Selkoe, D. J. (2003) Folding proteins in fatal ways. *Nature 426*, 900−904.
(5) Bonda, D. J., Wang, X., Perry, G., Nunomura, A., Tabaton, M., Zhu, X., and Smith, M. A. (2010) Oxidative stress in Alzheimer disease: a possibility for prevention. *Neuropharmacology 59*, 290−294.
(6) Maccioni, R. B., Farías, G., Morales, I., and Navarrete, L. (2010) The revitalized tau hypothesis on Alzheimer's disease. *Arch. Med. Res. 41* (3), 226−231.
(7) Greenough, M. A., Camakaris, J., and Bush, A. I. (2013) Metal dyshomeostasis and oxidative stress in Alzheimer's disease. *Neurochem. Int. 62* (5), 540−555.
(8) Scarpini, E., Scheltens, P., and Feldman, H. (2003) Treatment of Alzheimer's disease: current status and new perspectives. *Lancet Neurol. 2*, 539−547.
(9) Bartus, R. T., Dean, R. L., Pontecorvo, M. J., and Flicker, C. (1985) The cholinergic hypothesis: a historical overview, current perspective, and future directions. *Ann. N. Y. Acad. Sci. 444*, 332−358.
(10) Gold, P. E. (2003) Acetylcholine modulation of neural systems involved in learning and memory. *Neurobiol. Learn. Mem. 80*, 194−210.
(11) Holzgrabe, U., Kapková, P., Alptüzün, V., Scheiber, J., and Kugelmann, E. (2007) Targeting acetylcholinesterase to treat neurodegeneration. *Expert Opin. Ther. Targets 11*, 161−179.
(12) Hartmann, J., Kiewert, C., Duysen, E. G., Lockridge, O., Greig, N. H., and Klein, J. (2007) Excessive hippocampal acetylcholine levels in acetylcholinesterase-deficient mice are moderated by butyrylcholinesterase activity. *J. Neurochem. 100*, 1421−1429.
(13) Greig, N. H., Lahiri, D. K., and Sambamurti, K. (2002) Butyrylcholinesterase: an important new target in Alzheimer's disease therapy. *Int. Psychogeriatrics 14*, 77−91.
(14) Selkoe, D. J., and Hardy, J. (2016) The amyloid hypothesis of Alzheimer's disease at 25 years. *EMBO Mol. Med. 8*, 595−608.
(15) Hardy, J. (2009) The amyloid hypothesis for Alzheimer's disease: a critical reappraisal. *J. Neurochem. 110*, 1129−1134.
(16) O'Brien, R. J., and Wong, P. C. (2011) Amyloid precursor protein processing and Alzheimer's disease. *Annu. Rev. Neurosci. 34*, 185−204.
(17) Cheignon, C., Tomas, M., Bonnefont-Rousselot, D., Faller, P., Hureau, C., and Collin, F. (2018) Oxidative stress and the amyloid beta peptide in Alzheimer's disease. *Redox Biol. 14*, 450−464.
(18) Lobo, V., Patil, A., Phatak, A., and Chandra, N. (2010) Free radicals, antioxidants and functional foods: impact on human health. *Pharmacogn. Rev. 4*, 118−126.
(19) Uttara, B., Singh, A., Zamboni, P., and Mahajan, R. (2009) Oxidative stress and neurodegenerative diseases: A review of upstream and downstream antioxidant therapeutic options. *Curr. Neuropharmacol. 7*, 65−74.
(20) Patel, D. V., Patel, N. R., Kanhed, A. M., Patel, S. P., Sinha, A., Kansara, D. D., Mecwan, A. R., Patel, S. B., Upadhyay, P. N., Patel, K. B., Shah, D. B., Prajapati, N. K., Murumkar, P. R., Patel, K. V., and Yadav, M. R. (2019) Novel multitarget directed triazinoindole derivatives as anti-Alzheimer agents. *ACS Chem. Neurosci. 10*, 3635−3661.
(21) Chow, A. W. Polysubstituted *as*-triazino(5,6-*b*)indoles. U.S. Patent No. 3637687, 1972.
(22) Rydberg, P., Gloriam, D. E., Zaretzki, J., Breneman, C., and Olsen, L. (2010) SMARTCyp: A 2D method for prediction of cytochrome P450-mediated drug metabolism. *ACS Med. Chem. Lett. 1*, 96−100.
(23) Rydberg, P., Gloriam, D. E., and Olsen, L. (2010) The SMARTCyp cytochrome P450 metabolism prediction server. *Bioinformatics 26*, 2988−2989.
(24) Zaretzki, J., Matlock, M., and Swamidass, S. J. (2013) XenoSite: accurately predicting cyp-mediated sites of metabolism with neural networks. *J. Chem. Inf. Model. 53*, 3373−3383.
(25) Wang, Z. Sandmeyer isatin synthesis. In *Comprehensive Organic Name Reactions and Reagents*; Wiley: Hoboken, NJ, 2010; Vol. 3, pp 2467−2470, DOI: 10.1002/9780470638859.conrr557.
(26) Jeankumar, V. U., Alokam, R., Sridevi, J. P., Suryadevara, P., Matikonda, S. S., Peddi, S., Sahithi, S., Alvala, M., Yogeeswari, P., and Sriram, D. (2014) Discovery and structure optimization of a series of isatin derivatives as mycobacterium tuberculosis chorismate mutase inhibitors. *Chem. Biol. Drug Des. 83*, 498−506.
(27) Rosini, M., Simoni, E., Milelli, A., Minarini, A., and Melchiorre, C. (2014) Oxidative stress in Alzheimer's disease: are we connecting the dots? *J. Med. Chem. 57*, 2821−2831.
(28) Di, L., Kerns, E. H., Bezar, I. F., Petusky, S. L., and Huang, Y. (2009) Comparison of blood-brain barrier permeability assays: *in situ* brain perfusion, MDR1-MDCKII and PAMPA-BBB. *J. Pharm. Sci. 98*, 1980−1991.
(29) Di, L., Kerns, E. H., Fan, K., McConnell, O. J., and Carter, G. T. (2003) High throughput artificial membrane permeability assay for blood-brain barrier. *Eur. J. Med. Chem. 38*, 223−232.
(30) Protein Data Bank. www.rcsb.org/pdb/home/home.do (accessed Sept 2019).
(31) Crescenzi, O., Tomaselli, S., Guerrini, R., Salvadori, S., D'Ursi, A. M., Temussi, P. A., and Picone, D. (2002) Solution structure of the Alzheimer amyloid β-peptide (1−42) in an apolar microenvironment: similarity with a virus fusion domain. *Eur. J. Biochem. 269*, 5642−5648.
(32) *Qikprop*; Schrödinger, LLC: New York, NY, 2018-4 (accessed Sept 2019).
(33) Lipinski, C. A., Lombardo, F., Dominy, B. W., and Feeney, P. J. (2012) Experimental and computational approaches to estimate solubility and permeability in drug discovery and development settings. *Adv. Drug Delivery Rev. 64*, 4−17.
(34) Veber, D. F., Johnson, S. R., Cheng, H.-Y., Smith, B. R., Ward, K. W., and Kopple, K. D. (2002) Molecular properties that influence the oral bioavailability of drug candidates. *J. Med. Chem. 45*, 2615−2623.
(35) Kelder, J., Grootenhuis, P. D. J., Bayada, D. M., Delbressine, L. P. C., and Ploemen, J. P. (1999) Polar molecular surface as a dominating determinant for oral absorption and brain penetration of drugs. *Pharm. Res. 16*, 1514−1519.
(36) Pajouhesh, H., and Lenz, G. R. (2005) Medicinal chemical properties of successful central nervous system drugs. *NeuroRx 2*, 541−553.
(37) Waterhouse, R. N. (2003) Determination of lipophilicity and its use as a predictor of blood-brain barrier penetration of molecular imaging agents. *Mol. Imaging Biol. 5*, 376−389.
(38) Wang, Q., Rager, J. D., Weinstein, K., Kardos, P. S., Dobson, G. L., Li, J., and Hidalgo, I. J. (2005) Evaluation of the MDR-MDCK cell line as a permeability screen for the blood-brain barrier. *Int. J. Pharm. 288*, 349−359.
(39) Kaur, R., Mehan, S., and Kalra, S. (2015) Ameliorative treatment with ellagic acid in scopolamine induced Alzheimer's type memory and cognitive dysfunctions in rats. *Austin J. Clin. Neurol. 2*, 1053.
(40) Foyet, H. S., Ngatanko Abaïssou, H. H., Wado, E., Asongalem Acha, E., and Alin, C. (2015) Emilia coccinae (SIMS) G extract improves memory impairment, cholinergic dysfunction, and oxidative stress damage in scopolamine-treated rats. *BMC Complementary Altern. Med. 15*, 333.
(41) Rosenbrock, H., Desch, M., Kleiner, O., Dorner-Ciossek, C., Schmid, B., Keller, S., Schlecker, C., Moschetti, V., Goetz, S., Liesenfeld, K. H., and Fillon, G. (2018) Evaluation of pharmacokinetics and pharmacodynamics of BI 425809, a novel GLYT1 inhibitor: translational studies. *Clin. Transl. Sci. 11* (6), 616−623.
(42) Rosenbrock, H., Giovannini, R., Schmid, B., Kramer, G., Arban, R., Dorner-Ciossek, C., and Wunderlich, G. (2016) P4−010: Improving cognitive function in rodents via increasing glycine levels in brain by the novel glycine transporter-1 inhibitor BI 425809. *Alzheimer's Dementia 12*, P1018.

https://dx.doi.org/10.1021/acschemneuro.0c00448
ACS Chem. Neurosci. XXXX, XXX, XXX−XXX

(43) Zhang, L., Zhou, F. M., and Dani, J. A. (2004) Cholinergic drugs for Alzheimer's disease enhance *in vitro* dopamine release. *Mol. Pharmacol. 66*, 538−544.
(44) Chen, F. Z., Zhao, Y., and Chen, H. Z. (2019) MicroRNA-98 reduces amyloid β-protein production and improves oxidative stress and mitochondrial dysfunction through the notch signaling pathway via HEY2 in Alzheimer's disease mice. *Int. J. Mol. Med. 43*, 91−102.
(45) Ribeiro, N. M., da Silva, B. V., de Almeida Violante, F., Rezende, C. M., and Pinto, A. C. (2005) 5-Chloro- and 5,7-dichloroisatin by chlorination of isatin with trichloroisocyanuric acid. *Org. Prep. Proced. Int. 37*, 265−267.
(46) Seong, C. M., Park, W. K., Park, C. M., Kong, J. Y., and Park, N. S. (2008) Discovery of 3-aryl-3-methyl-1*H*-quinoline-2,4-diones as a new class of selective 5-HT_6 receptor antagonists. *Bioorg. Med. Chem. Lett. 18*, 738−743.
(47) Kollmar, M., Richard, P., and Stephan, R. (2002) 2-Amino-3-flurobenzoic acid. *Org. Synth. 79*, 196−198.
(48) Sai Prathima, P., Bikshapathi, R., and Rao, V. J. (2015) Synthesis of isatin derivatives under metal free conditions using hypervalent iodine. *Tetrahedron Lett. 56*, 6385−6388.
(49) Senadi, G. C., Hu, W. P., Boominathan, S. S. K., and Wang, J. J. (2015) Palladium(0)-catalyzed single and double isonitrile insertion: a facile synthesis of benzofurans, indoles, and isatins. *Chem. - Eur. J. 21*, 998−1003.
(50) Gianella-Borradori, M., Christou, I., Bataille, C. J. R., Cross, R. L., Wynne, G. M., Greaves, D. R., and Russell, A. J. (2015) Ligand-based virtual screening identifies a family of selective cannabinoid receptor 2 agonists. *Bioorg. Med. Chem. 23*, 241−263.
(51) Kanhed, A. M., Sinha, A., Machhi, J., Tripathi, A., Parikh, Z. S., Pillai, P. P., Giridhar, R., and Yadav, M. R. (2015) Discovery of isoalloxazine derivatives as a new class of potential anti-Alzheimer agents and their synthesis. *Bioorg. Chem. 61*, 7−12.
(52) Patel, D. V., Patel, N. R., Kanhed, A. M., Teli, D. M., Patel, K. B., Joshi, P. D., Patel, S. P., Gandhi, P. M., Chaudhary, B. N., Prajapati, N. K., Patel, K. V., and Yadav, M. R. (2020) Novel carbazole-stilbene hybrids as multifunctional anti-Alzheimer agents. *Bioorg. Chem. 101*, 103977.
(53) Morris, R. (1984) Developments of a water-maze procedure for studying spatial learning in the rat. *J. Neurosci. Methods 11*, 47−60.
(54) Wills, E. D. (1966) Mechanisms of lipid peroxide formation in animal tissues. *Biochem. J. 99*, 667−676.
(55) Misra, H. P., and Fridovich, I. (1972) The role of superoxide anion in the autoxidation of epinephrine and a simple assay for superoxide dismutase. *J. Biol. Chem. 247*, 3170−3175.
(56) Moron, M. S., Depierre, J. W., and Mannervik, B. (1979) Levels of glutathione, glutathione reductase and glutathione S-transferase activities in rat lung and liver. *Biochim. Biophys. Acta, Gen. Subj. 582*, 67−78.
(57) Monge-Acuña, A. A., and Fornaguera-Trías, J. (2009) A high performance liquid chromatography method with electrochemical detection of gamma-aminobutyric acid, glutamate and glutamine in rat brain homogenates. *J. Neurosci. Methods 183*, 176−181.
(58) Sivaraman, D., Panneerselvam, P., and Muralidharan, P. (2015) Revealing hallmark histology of hippocampus neurons in beta-amyloid induced Alzheimer's mice and investigation of neuroprotective effect of ipomoea aquatic forsk, an Indian medicinal herb. *J. Chem. Pharm. Res. 7*, 424−434.
(59) Sinha, A., Tamboli, R. S., Seth, B., Kanhed, A. M., Tiwari, S. K., Agarwal, S., Nair, S., Giridhar, R., Chaturvedi, R. K., and Yadav, M. R. (2015) Neuroprotective role of novel triazine derivatives by activating Wnt/β catenin signaling pathway in rodent models of Alzheimer's disease. *Mol. Neurobiol. 52*, 638−652.
(60) OECD (2002) Test No. 423: Acute Oral toxicity - Acute Toxic Class Method. https://www.oecd-ilibrary.org/environment/test-no-423-acute-oral-toxicity-acute-toxic-class-method_9789264071001-en (accessed May 2019).
(61) *Protein Preparation Wizard*; Epik, Schrödinger, LLC: New York, NY, 2016; Impact, Schrödinger, LLC, New York, NY, 2016; Prime, Schrödinger, LLC, New York, NY, 2020 (accessed December 2019).
(62) *LigPrep*; Schrödinger, LLC: New York, NY, 2018-4 (accessed Sept 2019).
(63) *Glide*; Schrödinger, LLC: New York, NY, 2018-4 (accessed Sept 2019).
(64) Sanner, M. F. (1999) Python: A programming language for software integration and development. *J. Mol. Graph. Model. 17*, 57−61.
(65) Morris, G. M., Huey, R., Lindstrom, W., Sanner, M. F., Belew, R. K., Goodsell, D. S., and Olson, A. J. (2009) AutoDock4 and AutoDockTools4: automated docking with selective receptor flexibility. *J. Comput. Chem. 30*, 2785−2791.
(66) Lindahl, E., Abraham, M., Hess, B., and van der Spoel, D. *GROMACS 2020.1 Source code*, version 2020.1 (accessed March 2020).
(67) Huang, J., Rauscher, S., Nawrocki, G., Ran, T., Feig, M., De Groot, B. L., Grubmüller, H., and MacKerell, A. D. (2017) CHARMM36m: An improved force field for folded and intrinsically disordered proteins. *Nat. Methods 14*, 71−73.
(68) Vanommeslaeghe, K., Acharya, C., Kundu, S., Zhong, S., Shim, J., Darian, E., Guvench, O., Lopes, P., Vorobyov, I., and Mackerell, A. D., Jr (2010) CHARMM general force field: a force field for drug-like molecules compatible with the CHARMM all-atom additive biological force fields. *J. Comput. Chem. 31*, 671−690.
(69) Yu, W., He, X., Vanommeslaeghe, K., and MacKerell, A. D. (2012) Extension of the CHARMM general force field to sulfonyl-containing compounds and its utility in biomolecular simulations. *J. Comput. Chem. 33*, 2451−2468.
(70) Mark, P., and Nilsson, L. (2001) Structure and dynamics of the TIP3P, SPC, and SPC/E water models at 298 K. *J. Phys. Chem. A 105*, 9954−9960.
(71) Bixon, M., and Lifson, S. (1967) Potential functions and conformations in cycloalkanes. *Tetrahedron 23*, 769−784.
(72) Darden, T., York, D., and Pedersen, L. (1993) Particle Mesh Ewald: An N·log(N) method for ewald sums in large systems. *J. Chem. Phys. 98* (12), 10089−10092.
(73) Turner, P. J. *XMGRACE*, Version 5.1.25; Center for coastal and land-margin research, oregon graduate institute of science and technology: Beaverton, OR, 2005 (accessed Feb - March, 2020 on Ubuntu platform).
(74) Rawat, R., Kant, K., Bhati, A., Dalchand Singh, U., Kumar, A., and Verma, S. M. HeroMDAnalysis: An automagical tool for MD simulation analysis 2020. http://www.heromdanalysis.wordpress.com (accessed Feb - March, 2020).

https://dx.doi.org/10.1021/acschemneuro.0c00448
ACS Chem. Neurosci. XXXX, XXX, XXX−XXX